

## 2MASS Observations of the Perseus, Orion A, Orion B, and Monoceros R2 Molecular Clouds

John M. Carpenter

California Institute of Technology, Department of Astronomy, MS 105-24,  
Pasadena, CA 91125; email: jmc@astro.caltech.edu

### ABSTRACT

We use the *2MASS* Second Incremental Release Point Source Catalog to investigate the spatial distribution of young stars in the Perseus, Orion A, Orion B, and MonR2 molecular clouds. After subtracting a semi-empirical model of the field star contamination from the observed star counts, stellar surface density maps are used to identify compact clusters and any stellar population found more uniformly distributed over the molecular cloud. Each cloud contains between 2 to 7 clusters, with at least half of the cluster population found in a single, rich cluster. In addition, a distributed stellar population is inferred in the Orion A and MonR2 molecular clouds within the uncertainties of the field star subtraction with a surface density between  $0.013 - 0.083 \text{ arcmin}^{-2}$ . Sensitivity calculations suggest, however, that the number of stars in the distributed population may be underestimated by a factor of 2 or more if stars have been forming with a Miller-Scalo IMF at a constant star formation rate for longer than 10 Myr. After considering the possible evolutionary status of the distributed population, the global star formation efficiency implied by the sum of the distributed and cluster populations ranges between 1-9% among the four clouds. The fraction of the total stellar population contained in clusters for the nominal extinction model ranges from  $\approx 50\text{-}100\%$  if the distributed population is relatively young ( $< 10$  Myr), to  $\approx 25\text{-}70\%$  if it is relatively old ( $\approx 100$  Myr). The relatively high fraction of stars contained in clusters regardless of the age of the distributed population, in conjunction with the young ages generally inferred for embedded clusters in nearby molecular clouds, indicates that a substantial fraction of the total stellar population in these regions has formed within the past few million years in dense clusters. This suggests that either the star formation rate in each these clouds has recently peaked if one assumes clouds have ages  $> 10$  Myr, or molecular clouds are younger than typically thought if one assumes that the star formation rate has been approximately constant in time.

*Subject headings:* stars: formation — stars: pre-main-sequence — ISM: individual:(Perseus, Orion A, Orion B, MonR2)

## 1. Introduction

Nearby star forming regions display a continuum of properties, ranging from isolated young stellar objects and loose “aggregates” (Gomez et al. 1993; Strom, Strom, & Merrill 1993) to dense clusters containing hundreds if not thousands of stars within parsec sized regions (Lada et al. 1991; Carpenter et al. 1997; Hillenbrand & Hartmann 1998). The diverse range of observed stellar environments reflect the various physical processes that initiate star formation over the lifetime of molecular clouds. In principle, the predominant mechanisms that lead to star formation can be inferred by reconstructing the star formation rate in molecular clouds as a function of time and stellar mass. While a comprehensive picture of how star formation evolves in time requires obtaining masses and ages for the individual stars that have formed within a cloud, constraints on the star formation history can nonetheless be obtained from a census of the embedded stellar population to establish the number of stars that have formed and where in the cloud they tend to be located.

The stellar population associated with a cloud is most often identified using large scale surveys for an emission feature commonly associated with pre-main-sequence stars, such as far-infrared emission (e.g. Beichman et al. 1986), near-infrared excesses (e.g. Cambrésy et al. 1998), H $\alpha$  (e.g. Nakano, Wiramihardja, & Kogure 1995), or X-rays (e.g. Walter et al. 1988). While such studies generally produce reliable catalogs of young stellar objects, they may not provide a complete census of the stellar population in molecular clouds. Surveys for far-infrared emission, near-infrared excesses, and H $\alpha$  in particular generally detect pre-main-sequence objects surrounded by an optically thick circumstellar disk or envelope. The evolution of circumstellar material as a function of stellar age and mass remains poorly quantified, which makes it difficult to infer the extent of the stellar population not currently in this phase of stellar evolution and not detectable by these diagnostics. Indeed, X-ray observations, which probe stellar chromospheric activity and can readily detect stars as old as  $\approx 100$  Myr in nearby ( $\lesssim 200$  pc) star forming regions, have detected a widespread population of objects in and around molecular clouds. The interpretation of the X-ray results remain controversial, though, as the spatially extended X-ray population may represent older pre-main-sequence stars that have dispersed from molecular clouds, stars that formed in surrounding clouddlets (Feigelson 1996), or young main sequence stars that have formed in the solar neighborhood in the past 100 Myr (Briceño et al. 1997; Favata, Micela, & Sciortino 1997). Furthermore, X-ray observations in the pre-Chandra era lack the required combination of sensitivity, coverage, and angular resolution to provide an accurate census of the stellar population contained in both isolated star forming regions and dense clusters over entire molecular clouds.

An alternative approach to infer the underlying stellar population in molecular clouds is to statistically determine the excess number of stars observed toward the cloud relative to the expected field star contribution. Such star count techniques are best suited for molecular clouds located at high Galactic latitudes where the field star contamination is less severe, and for near-infrared wavelength surveys where embedded stars are more readily detected. While near-infrared star count analyses have the obvious limitation that individual young stellar objects cannot be uniquely

identified for further study, they represent a powerful probe of the stellar population in that near-infrared emission generally originates from the stellar photosphere (except for the heavily accreting objects). The intrinsic brightness of a star then depends foremost on the stellar mass (and age for pre-main-sequence objects), and the parameter space probed by a set of observations can be estimated with the aid of pre-main-sequence evolutionary models. Further, current observations are generally sensitive to stars spanning a broad range of masses and ages, including objects in nearby molecular clouds with masses below the hydrogen burning limit, and have the angular resolution needed to resolve many of the stars in dense clusters. Thus near-infrared star count studies have the potential obtain a more unbiased census of the embedded stellar population in molecular clouds.

The first extensive near-infrared observations to statistically characterize the spatial distribution of young stars in a molecular cloud was the  $K$  band survey of Orion B (L1630) by Lada et al. (1991; see also Li, Evans, & Lada 1997). Surveys of other regions with similar aims have since been conducted for Orion A (L1641; Strom, Strom, & Merrill 1993), NGC 2264 (Lada, Young, & Greene 1993; Piche 1993), the Rosette (Phelps & Lada 1997), NGC 1333 (Lada, Alves, & Lada 1996), and Ophiuchus (Strom, Kepner, & Strom 1995; Barsony et al. 1997) among others (see recent reviews by Allen & Hillenbrand 2000; Meyer & Lada 2000; Clarke, Bonnell, & Hillenbrand 2000). A synthesis of these results suggest that more than half of the stellar population in molecular clouds is contained in clusters with various sizes and densities (Clarke, Bonnell, & Hillenbrand 2000). However, most near-infrared observations to date cover only a fraction of the total cloud area and nearly all have been predisposed toward regions within clouds known *a priori* to contain prominent star formation activity (and likely clusters). Thus current near-infrared observations do not accurately characterize the spatial distribution of stars over entire molecular clouds.

The 2 Micron All Sky Survey (*2MASS*) removes many of the limitations of prior observations and has provided the first sensitive, uniformly calibrated  $J$ ,  $H$ , and  $K_s$  near-infrared survey over entire molecular clouds. In this paper, we analyze data from the *2MASS* Second Incremental Release to investigate the spatial distribution of young stars in the Perseus, Orion A, Orion B, and Monoceros R2 (MonR2) molecular clouds in order to determine the relative importance of cluster and isolated stellar systems. These clouds were chosen for this study since they are nearby with distances less than 1 kpc to maximum sensitivity to the low mass stellar population, are located at high Galactic latitudes ( $|b| > 10^\circ$ ) to minimize field star contamination, and have available  $^{13}\text{CO}$  maps that are required for the analysis presented here. The results from this study are presented as follows. In Section 2, we review the characteristics of the *2MASS* data and select a subset of the point source catalog for analysis. In Section 3, the near-infrared star counts toward the Perseus, Orion A, Orion B, and MonR2 molecular clouds are used to identify any cluster and distributed stellar populations. The implications of these results for the star formation history of molecular clouds is discussed in Section 4, and the conclusions are summarized in Section 5.

## 2. 2MASS Data

The near-infrared data analyzed in this study were obtained from the *2MASS* Second Incremental Data Release. The observational goal of *2MASS* is to survey  $>95\%$  of the sky simultaneously in the  $J$ ,  $H$ , and  $K_s$  bands. The data are obtained by scanning a series of  $8.5' \times 6^\circ$  long tiles aligned in declination. Each position in a tile is observed first with a short, 51 msec integration to recover photometry for bright stars (between  $\approx 5\text{-}8^m$ ), and then with a relatively long, 1.3 sec integration for deeper photometry. Adjacent images within a tile overlap such that each position on the sky is nominally observed 6 times. The pixel scale of the observations is  $2''$ , but since overlapping images within a tile are designed to subsample the raw camera pixels, the coadded images produced in data reduction from the long integration frames have a pixel scale of  $1''$ . The *2MASS* Second Incremental Release Point Source Catalog contains a list of positions and magnitudes for point sources in  $\approx 47\%$  of the sky that have a photometric uncertainty  $\leq 0.155^m$  (i.e. a signal to noise ratio  $\geq 7.0$ ) in at least one of the three observed bands. This study analyzes a subset of the catalog that includes the Perseus, Orion A, Orion B, and MonR2 molecular clouds. At the time of the Second Incremental Release, *2MASS* data are available for the entire area of the MonR2 and Orion A molecular clouds,  $\approx 80\%$  of Perseus, and  $\approx 70\%$  of Orion B. The galactic coordinates of these clouds and their adopted distances are summarized in Table 1.

The *2MASS* point source data need to be analyzed at magnitude limits bright enough to ensure uniform completeness across the region studied. The magnitude thresholds for the three bands were set by computing as a function of magnitude the average signal to noise ratio and the fraction of stars that have a signal to noise ratio  $\geq 10$  for point sources between Galactic longitudes of  $130^\circ$  and  $250^\circ$  and Galactic latitudes of  $-50^\circ$  and  $+50^\circ$ . Based on this analysis, the faint magnitudes thresholds for analyzing the star counts were set at  $15.8^m$ ,  $14.9^m$ , and  $14.3^m$  at  $J$ ,  $H$ , and  $K_s$  band respectively. At these thresholds, the average signal to noise for the point sources is between 14-15, and greater than 99%, 99%, and 97% of the sources at these magnitude limits have a photometric uncertainty corresponding to a signal to noise ratio  $\geq 10$ . Stars brighter than  $\approx 5^m$  are saturated even in the short integration data, and as a conservative limit, it was required that stars be fainter than  $6.0^m$  in the appropriate band to be included in the analysis. At the galactic coordinates of the clouds studied here, the average source densities at the faint magnitude thresholds are  $\lesssim 2 \text{ arcmin}^{-2}$ , which implies a typical source separation of  $\gtrsim 40''$ . Thus source identification will only be confusion limited in the densest clusters which can have substantially higher surface densities than these average values.

Individual survey tiles may have poorer sensitivity than the adopted magnitude thresholds if spatial structure in the sky background from airglow emission added substantially to the sky noise (especially at  $H$  band) at the time of the observation or if the sky background was much higher than average (especially at  $K_s$  band). Data adversely affected by airglow were identified and removed in the present analysis by finding all tiles in the Second Incremental Release Scan Database in which the observed sky noise was 20% higher than the expected noise computed from the sky background level. The percentage of the total number of tiles ( $\approx 9400$  total) removed due

to this criteria amounted to 0%, 8%, 0.1% at  $J$ ,  $H$ , and  $K_s$  band respectively. To remove lower sensitivity data because of a high sky background level, tiles in which the average signal to noise ratio is less than 10.0 at the adopted magnitude thresholds were also discarded. The percentage of tiles removed by this criteria were 0.14%, 0.07%, and 0.25% at  $J$ ,  $H$ , and  $K_s$  band.

Finally, some point sources identified around bright stars ( $m \lesssim 9.5^m$ ) were omitted when drafting the Second Incremental Release Catalogs so that image artifacts from bright objects would not reduce the data reliability. The masked areas are primarily due to diffraction spikes and circular regions centered on bright saturated stars. The dimensions of these masks depend on the magnitude of the bright star and effectively create holes in the star count maps. Using the quantitative description of these masks provided in the *2MASS* Explanatory Supplement, the fraction of each pixel in the star count map that has been partially or completely masked was computed as a function of magnitude and was used to correct the star counts maps on a pixel by pixel basis.

### 3. Analysis

A  $K_s$  band stellar surface density map for the area between Galactic longitudes of  $130^\circ$  and  $250^\circ$  and Galactic latitudes of  $-40^\circ$  and  $+40^\circ$  is shown in Figure 1. The surface density map was generated by binning stars with  $K_s$  band magnitudes between  $6.0^m$  and  $14.3^m$  in  $5' \times 5'$  cells. The Galactic Plane is clearly visible as a band of stars extending across the center of the image. The location of the Perseus, Orion A, Orion B, and MonR2 molecular clouds are labeled in Figure 1, but because of the low  $K_s$  band extinction, the outline of the clouds are only faintly seen in absorption against the backdrop of field stars. To gain a better perspective on the location of various molecular clouds, Figure 2 presents a map of the average  $J - K_s$  stellar color for the same region shown in Figure 1. Large  $J - K_s$  colors, represented by darker gray scales in Figure 2, are attributed to background field stars and embedded young stellar objects reddened by dust associated with molecular clouds. The Taurus, Perseus, Orion A, Orion B, and MonR2 molecular clouds are clearly visible in Figure 2, as well as numerous clouds in the Galactic Plane. The outline of the clouds agree well with that inferred from optical star counts (Cambrésy 1999) and far-infrared emission (Reach, Wall, & Odegard 1998).

The observed star counts toward a molecular cloud consist of unreddened foreground field stars, background field stars reddened by dust within the cloud, and young stars associated with the cloud itself. The spatial distribution of young stars in the cloud can then be obtained by removing the field stars from the star count map. Ideally one would like to specifically identify the individual young stars so that they can be furthered studied. However, near-infrared photometry alone cannot uniquely distinguish field stars from the stellar population associated with the cloud. Stars with relatively blue near-infrared colors can either be foreground field stars, background field stars appearing through holes in the cloud, or young stars on the surface of the cloud. Similarly, red stars can either be background reddened field stars or pre-main-sequence objects embedded in the cloud. The degeneracy between the field and embedded stellar population can be only

partially reduced by considering both the magnitudes and colors. Therefore, instead of attempting to uniquely identify which stars are associated with the cloud, the embedded stellar population was inferred statistically by first constructing a semi-empirical model of the expected field star surface density toward the cloud, and then subtracting the field star model from the observed stellar surface density map. In principle, the star count analysis can be done by simultaneously analyzing the five observable quantities for each star (i.e. Galactic longitude and latitude and the observed  $J$ ,  $H$ , and  $K_s$  band magnitudes). In the analysis conducted here, the three near-infrared bands are analyzed separately to determine if each band provides a consistent picture of the embedded stellar population. The following sections describe how the semi-empirical field star model was generated using *2MASS* observations of regions away from the molecular clouds and published  $^{13}\text{CO}$ (1–0) maps as a tracer of the cloud extinction. The field star subtracted stellar surface density map is then used to identify stellar clusters and any stars distributed more uniformly throughout the molecular cloud.

### 3.1. Semi-Empirical Field Star Model

The expected number of field stars toward the molecular clouds in the absence of extinction from the cloud itself was estimated using *2MASS* observations of regions outside the molecular cloud boundaries. This was accomplished by fitting Legendre polynomials as a function of Galactic longitude and latitude to  $J$ ,  $H$ , and  $K_s$  surface density maps for the region between  $\ell = 130^\circ$  to  $240^\circ$  and  $b = -35^\circ$  to  $-7^\circ$  binned in  $5' \times 5'$  cells (see Figure 1). This bin size was chosen so that large scale gradients in the field star counts are well resolved while maintaining a manageable image size. A global fit was performed to the large scale surface density maps as opposed to fitting a localized region around each cloud since several blocks of *2MASS* tiles were not available at the time of this study, especially near the Orion B molecular cloud. Without these tiles, a localized polynomial fit is poorly constrained near the cloud boundaries. Lines of sight in the surface density map that pass through an obvious stellar cluster (see Figure 1) or that intercept a molecular cloud as traced by molecular emission (Maddalena et al. 1986; Dame et al. 1987; Bally et al. 1987; Miesch & Bally 1994; Padoan et al. 1999) or red  $J - K_s$  colors (see Figure 2) were excluded from the fit. At least a  $0.5^\circ$  border around each cloud was also excluded which prevented any potential young stars surrounding the clouds from influencing the polynomial fit. The remaining  $\approx 180,000$  pixels in each surface density map were then fitted with Legendre polynomials. The order of the polynomial fit was increased until the systematics in the residuals as a function of position were no longer evident. A seventh order polynomial fit in both longitude and latitude were ultimately used. The results from the polynomial fit are examined in Figure 3, which shows as a function of Galactic latitude the observed mean stellar surface density, the mean residuals after subtracting the polynomial fit, and the RMS in the residuals for each band. The RMS of the residuals varies between  $\approx 0.1\text{--}0.3 \text{ arcmin}^{-2}$  depending on the band and the Galactic latitude, and is consistent with that expected from Poisson statistics within the  $5' \times 5'$  bin sizes.

The polynomial fit described above was interpolated to yield the expected surface density of field stars as a function of Galactic longitude and latitude toward the molecular clouds in the absence of extinction from the cloud itself. The uncertainties associated with interpolating the polynomial fit were assessed by performing a similar fit to star counts at the same Galactic longitude but at positive latitudes where there are essentially no clouds (see Figure 2). The molecular clouds masks used in fitting the star counts at negative latitude were also used at positive latitudes in order to preserve the geometry and number of masked regions. The accuracy of the interpolated polynomial fit was assessed by subtracting the fit from the observed star counts in the masked regions and computing the RMS of the residuals in areas  $6 \text{ deg}^2$  in size, which is a typical area of the larger clouds analyzed here. It was found that the average difference over this sized region between the interpolated fit and the observed star counts is  $\lesssim 0.003 \text{ arcmin}^{-2}$  in each band with a RMS deviation of  $\approx 0.002 \text{ arcmin}^{-2}$ .

Dust within the molecular clouds obscures background field stars and depresses the total field star counts relative to the interpolated polynomial fit. The number of field stars that are obscured depends on the extinction along the line of sight and the frequency distribution of magnitudes for the background field star population, as foreground field stars will not be further reddened by the cloud. The extinction as a function of position through the molecular clouds was estimated using published  $^{13}\text{CO}$  maps of the MonR2, Orion A, Orion B, and Perseus molecular clouds kindly provided by J. Bally (see Padoan et al. 1999; Miesch & Bally 1994; Bally et al. 1987). These maps have a full-width-at-half-maximum beam size of  $100''$  with a sampling of  $60''$ . While the molecular gas will contain substructure within the  $100''$  beam, these maps resolve the large scale structural features present in these clouds and should accurately trace the global spatial distribution of extinction.

Assuming that the  $^{13}\text{CO}(1-0)$  emission is optically thin and in Local Thermodynamic Equilibrium, the  $^{13}\text{CO}$  column density can be estimated from the  $J=1-0$  integrated intensity using the formula

$$N(^{13}\text{CO}) = 4.57 \times 10^{13} T_{\text{ex}} e^{5.287/T_{\text{ex}}} \int \frac{T_{\text{mb}} \Delta v}{\text{K km s}^{-1}} \text{ cm}^{-2}, \quad (1)$$

where  $T_{\text{ex}}$  is the excitation temperature and  $\int T_{\text{mb}} \Delta v$  the integrated  $^{13}\text{CO}(1-0)$  intensity. The derived  $^{13}\text{CO}$  column densities will be in error by less than a factor of 2 by assuming  $T_{\text{ex}}=10 \text{ K}$  as long as the actual excitation temperature is less than 30 K. Such high excitation temperatures are expected only toward the embedded OB stars which occupy a small fraction of the total cloud area in any of these regions. The  $^{13}\text{CO}$  column densities can be converted into visual extinctions using the empirical  $N(^{13}\text{CO})-A_V$  correlations that have been observed in many clouds (Frerking, Langer, & Wilson 1982; Bachiller & Cernicharo 1986; Langer et al. 1989; Lee, Snell, & Dickman 1994; Lada et al. 1994; Hayakawa et al. 1999). These studies have shown that the ratio of  $N(^{13}\text{CO})$  to  $A_V$  is typically within the range of  $\approx 1.5 - 2.5 \times 10^{15} \text{ cm}^{-2} \text{ mag}^{-1}$  and that  $^{13}\text{CO}$  is detectable only when the visual extinction reaches a threshold value of  $\approx 0.5-1.5$  magnitude due to photodissociation of the molecules at low column densities (Frerking, Langer, & Wilson 1982). To determine the sensitivity of the field star model on the derived extinctions, three different set of assumptions were

adopted to convert the  $^{13}\text{CO}$  column densities into visual extinctions. The “nominal” extinction model assumes a  $N(^{13}\text{CO})/A_V$  ratio of  $2.18 \times 10^{15} \text{ cm}^{-2} \text{ mag}^{-1}$  as derived by Lada et al. (1994) and that the extinction needed to detect  $^{13}\text{CO}(1-0)$  is  $A_V = 1^{\text{m}}$ . This calibration was adopted since it has the best statistical accuracy among published observations and the parameters are in the middle of values generally observed in molecular clouds. Similarly, a “low” extinction model was derived by assuming a  $N(^{13}\text{CO})/A_V$  ratio of  $2.5 \times 10^{15} \text{ cm}^{-2} \text{ mag}^{-1}$  and a visual extinction threshold of  $0.5^{\text{m}}$ , and a “high” extinction model was obtained by assuming a  $N(^{13}\text{CO})/A_V$  ratio of  $1.5 \times 10^{15} \text{ cm}^{-2} \text{ mag}^{-1}$  and a visual extinction threshold of  $1.5^{\text{m}}$ . The low and high extinction models adopt parameters at the extrema of the observed values and are assumed to represent the plausible range of visual extinction and are not formal  $1\sigma$  confidence intervals. The masses of the clouds under these three extinction assumptions are summarized in Table 1.

The observed correlation between  $^{13}\text{CO}$  column density and visual extinction is valid for  $A_V \leq 5^{\text{m}}$  (Lada et al. 1994). For  $A_V \gtrsim 10^{\text{m}}$ , the  $^{13}\text{CO}(1-0)$  emission is saturated and is not a reliable tracer of the extinction. The  $^{13}\text{CO}$  maps used here have a  $3\sigma$  detection level corresponding to a visual extinction of  $\approx 0.2^{\text{m}}$  (not including the visual extinction threshold) for the nominal extinction model. The fraction of the Perseus, Orion A, Orion B, and MonR2 cloud area with an inferred visual extinction  $\leq 5^{\text{m}}$  is 95%, 88%, 92%, and 98% respectively. Therefore,  $^{13}\text{CO}(1-0)$  emission should accurately trace the extinction over nearly the entire cloud area.

The last step in constructing the field star model is to estimate the fraction of background field stars that become obscured by dust within the molecular clouds. This fraction was estimated using the extinction maps described above and the Wainscoat et al. (1992) Galactic star count model. This model agrees with the observed star counts to within 15% for high Galactic latitude regions ( $|b| > 5^{\circ}$ ) that do not contain additional reddening along the line of sight from molecular clouds. Since Perseus, Orion A, Orion B, and MonR2 are all located at Galactic latitudes between  $-20^{\circ}$  and  $-10^{\circ}$ , we expect that this model should provide an accurate estimate of the fraction of field stars that are foreground to the molecular clouds. The Wainscoat et al. (1992) model predicts that the fraction of the total field star counts contributed by foreground field stars ranges from 0.05-0.08 in Perseus to 0.2-0.4 in MonR2 in the  $J$ ,  $H$ , and  $K_s$  bands. The predicted absolute level of the foreground field star contamination is between  $0.04 \text{ arcmin}^{-2}$  (Perseus) and  $\lesssim 0.3 \text{ arcmin}^{-2}$  (MonR2).

For each line of sight toward the molecular clouds with a  $^{13}\text{CO}(1-0)$  detection, the expected number of field stars were computed using the Wainscoat star model with and without the  $^{13}\text{CO}$  derived extinction added at the appropriate cloud distance. The fraction of the field star population in this model that are reddened to magnitudes outside the adopted thresholds (see Section 2) was then computed, and the expected field star contribution inferred from the polynomial fits was reduced by the same fraction for that line of sight. Thus the total number of unreddened field stars is still determined by *2MASS* observations, and only the relative fraction of field stars obscured by extinction from dust in molecular clouds is model dependent. In performing the calculations,

we adopted the interstellar reddening vector from Cohen et al. (1981) and the cloud distances summarized in Table 1.

Uncertainties in the molecular cloud distances and the three dimensional structure of the clouds contribute to uncertainties in the field star model since extinction from the molecular cloud is applied only to the background field stars. The distance dependent uncertainties on the field star subtraction were quantified using the Wainscoat et al. (1992) star count model. Adopting an average visual extinction of  $3^m$  as implied by the  $^{13}\text{CO}$  maps, the  $K$  band field star surface density computed from the Wainscoat model will vary by  $\approx \pm 0.002 \text{ arcmin}^{-2}$  for Perseus,  $\pm 0.004 \text{ arcmin}^{-2}$  for Orion A and Orion B, and  $\pm 0.014 \text{ arcmin}^{-2}$  for MonR2 by changing the cloud distance by  $\pm 20\%$  from the nominal assumed value. The corresponding uncertainties at  $J$  and  $H$  bands are higher by a factor of  $\approx 2\text{-}3$ . The uncertainties are largest for MonR2 since it is the most distant cloud analyzed here and the foreground field stars contain a greater fraction of the total field star counts than toward Perseus, Orion A, or Orion B. In addition, since molecular clouds are three dimensional structures, there may be systematic variations in the distances to different parts of the cloud. For the Orion molecular clouds in particular, Brown, de Geus, & de Zeeuw (1994) argue that the near edge of the Orion A and Orion B molecular clouds is at a distance of  $\approx 320 \text{ pc}$ , and the far edge is at a distance of  $\approx 500 \text{ pc}$ . The difference in the field star model between these two distances for a visual extinction of  $3^m$  is  $\approx 0.006 \text{ arcmin}^{-2}$ .

### 3.2. Field Star Subtracted Surface Density Maps

The stellar population associated with the cloud can be inferred by subtracting the field star model from the observed star counts. Instead of using the binned star count maps that were produced for the field star polynomial fit, (e.g. Figure 1), stellar surface density maps were regenerated for the molecular clouds from the observed star counts using adaptive kernel density estimation (Silverman 1986). In this method, each star is represented by a kernel function, such as a gaussian, where the width of the kernel depends on the local stellar density as described below. The sum of the individual kernel functions yields the stellar density map for the cloud. The advantage of adaptive kernel density estimation compared to a fixed kernel size or a binned star count map is that the resolution of the map varies with the local stellar density which enables compact clusters to be more readily identified.

The kernel width for each star was computed using the procedure outlined in Silverman (1986). First, a pilot stellar density map,  $\tilde{f}(\ell, b)$ , was constructed using the standard kernel density estimate as

$$\tilde{f}(\ell, b) = \sum_{i=1}^n K_i(h, \ell, b), \quad (2)$$

where  $h$  is the bandwidth that controls the amount of smoothing,  $K$  is the kernel function, and  $n$  is the number of stars. The results are not sensitive to the choice of the Kernel function, and a

radially symmetric gaussian kernel was adopted such that

$$K_i(h, \ell, b) = \frac{\cos b_i}{2\pi h^2} e^{-\frac{(\ell-\ell_i)^2 \cos^2 b_i}{2h^2}} e^{-\frac{(b-b_i)^2}{2h^2}}. \quad (3)$$

For the pilot density estimate, the bandwidth,  $h$ , was fixed at the angular size corresponding to 0.25 pc in anticipation that clusters and their associated dense molecular cores have typical sizes of  $\approx 1$  pc. A local bandwidth,  $\lambda_i$ , was then computed for each star as

$$\lambda_i = [\tilde{f}(\ell_i, b_i)/g]^{-\alpha}, \quad (4)$$

where  $g$  is the geometric mean of  $\tilde{f}(\ell_i, b_i)$ ,  $i = 1, n$ . Following Silverman (1986),  $\alpha$  was set to be 0.5. Thus in regions of low stellar surface density such that  $\tilde{f}(\ell, b)$  is small, the local bandwidth,  $\lambda$ , is relatively large and the data are heavily smoothed. Conversely, in regions of high density such that  $\tilde{f}(\ell_i, b_i)$  is large,  $\lambda$  is relatively small and the data are smoothed less. The adaptive kernel density estimate was then computed as

$$\hat{f}(\ell, b) = \sum_{i=1}^n K_i(h\lambda_i, \ell, b). \quad (5)$$

As for the pilot density estimate, the bandwidth,  $h$ , was chosen to be 0.25 pc. The expected number of field stars for each pixel in the map (see Section 3.1) was then subtracted from the adaptive kernel surface density image to obtain the stellar population associated with the cloud.

### 3.3. Stellar Clusters

$K_s$  band surface density maps for the Perseus, Orion A, Orion B, and MonR2 molecular clouds are presented in Figures 4–7 along with corresponding *IRAS* 60 $\mu$ m images,  $^{13}\text{CO}$ (1–0) integrated intensity maps (Bally et al. 1987; Miesch & Bally 1994; Padoan et al. 1999), and an image of the average  $J - K_s$  color for points sources in the *2MASS* Second Incremental Release. Based on the extent of the molecular clouds indicated by the  $^{13}\text{CO}$  images, the *2MASS* observations at the time of this study were not available for the southern portion of the Perseus molecular cloud and the northern third of the Orion B molecular cloud. Further, the Orion A  $^{13}\text{CO}$  map from Bally et al. (1987) does not encompass the full extent of the molecular emission near  $\ell = 214^\circ$  (see Nagahama et al. 1998).

Stellar clusters were identified by forming closed contours at the  $2\sigma$  level above the local background level in the field star subtracted density maps. The noise in the star counts,  $\sigma$ , was determined by assuming Poisson statistics for the field stars at the appropriate latitude and longitude. Clusters are defined as closed contours that have a peak stellar surface density  $\geq 6\sigma$  and a total number of stars within the closed contour  $\geq 4\sigma$  with respect to the expected field star population. These thresholds are arbitrary, and were selected using lines of sight away from the molecular cloud as a control field that should be dominated by field star population and contain few if any clusters.

While the  $6\sigma$  peak density requirement biases the algorithm from finding extended, low density clusters, the resulting list of the clusters should be fairly reliable.

The clusters identified in the field star subtracted density map are listed in Table 2 along with the number of cluster members, the angular area within the  $2\sigma$  contour, and any associations with known star forming regions. All of the identified clusters are located at least partially in projection against the molecular cloud boundaries. Three of the clusters in Orion A are outside the spatial extent of the  $^{13}\text{CO}$  image. As discussed further below, lower limits to the cluster membership are provided for a few clusters since part of the cluster area has been masked in the *2MASS* Point Source Catalog due to neighboring bright stars. The clusters are labeled in the surface density maps in Figures 4–7, and contour maps of the  $K_s$  stellar surface for each cluster are presented in Figure 8. The major axis of the cluster measured at the  $2\sigma$  contour level ranges from  $\approx 1$  pc to  $\approx 16$  pc for the Orion Nebula Cluster (ONC).  $J - H$  vs.  $H - K_s$  color-color diagrams for stars within the projected area of each cluster are shown in Figure 9. Each cluster contains a number of stars with red near-infrared colors, supporting the notion that these clusters are indeed embedded within the molecular clouds.

Most of the clusters shown in Figure 8 have been previously identified and studied. In the Perseus molecular cloud, the IC 348 cluster has been the subject of several photometric and spectroscopic investigations (Lada & Lada 1995; Herbig 1998; Luhman et al. 1998; Luhman 1999). In the Orion A molecular cloud, the ONC (Jones & Walker 1988; Prosser et al. 1994; Ali & Depoy 1995; Hillenbrand 1997) is by the far largest, richest cluster identified here and extends for  $\approx 2^\circ$  (16 pc) along a filament of molecular gas prevalent in molecular line (Bally et al. 1987; Tatematsu et al. 1998; Nagahama et al. 1998) and dust continuum (Lis et al. 1998; Johnstone & Bally 1999) images. The boundaries of the ONC as defined here include the L1641N cluster (Strom, Strom, & Merrill 1993; Chen et al. 1993; Chen & Tokunaga 1994) and a couple of stellar density enhancements associated with *IRAS* point sources (Chen & Tokunaga 1994). In the Orion B molecular cloud, NGC 2024 (Lada et al. 1991; Comerón, Rieke, & Rieke 1996; Meyer 1996) and NGC 2068 (Lada et al. 1991) are identified as clusters, although NGC 2068 is at the edge of the density map and has not yet been completely imaged by *2MASS*. Finally, the major cluster identified in the MonR2 molecular cloud is the MonR2 cluster itself (Aspin & Walther 1990; Howard, Pipher, & Forrest 1994; Carpenter et al. 1997).

The number of cluster members listed in Table 2 are lower limits to the total cluster membership in these clouds. As with any survey, the completeness of the cluster membership is limited by the ability to resolve stars in crowded regions, the sensitivity of the observations to stars of various ages and masses, the high extinction in many clusters that may obscure some stars, and the difficulties in detecting point sources against bright nebular backgrounds that often accompany young star forming regions. Further, as a feature of the *2MASS* Second Incremental Release Point Source Catalog, part of the cluster area in IC 348, L 1641 C, the ONC, and NGC 2024 have been masked out due to the presence of nearby bright stars (see Figure 8). The fraction of the cluster area masked out in the IC 348, L 1641 C, and ONC clusters is estimated to be  $\approx 10\%$ ,  $5\%$ , and  $5\%$  respectively.

The masked region in the ONC includes the dense Trapezium region that contains  $\approx 600$  hundred stars brighter than  $K=14^m$  within the central  $5' \times 5'$  of the cluster (McCaughrean & Stauffer 1994; Hillenbrand & Carpenter 2000). To assess the fraction of the cluster population masked out in NGC 2024, the *2MASS* observations were compared with the NGC 2024  $K$  band survey by Lada et al. (1991), which has comparable resolution and sensitivity as the *2MASS* observations. They identified 309 stars within the cluster boundaries, compared to  $>201$  stars found here.

The density and molecular cloud maps presented in Figures 4-7 show that the *2MASS* observations at the time of this study were not complete toward the Perseus and Orion B molecular clouds. The prominent star forming regions contained within these unscanned areas include the NGC 1333 cluster in Perseus (Aspin, Sandell, & Russell 1994; Lada, Alves, & Lada 1996; Aspin & Sandell 1997), the NGC 2071 cluster in Orion B (Lada et al. 1991), and the remaining part of NGC 2068 in Orion B. Previous observations with comparable sensitivity and resolution as the *2MASS* data suggest that the NGC 1333 cluster contains  $\approx 94$  stars (Lada, Alves, & Lada 1996) and NGC 2071  $\approx 105$  stars (Lada et al. 1991). The NGC 2068 cluster contains  $\approx 147$  stars in addition to those already found identified (Lada et al. 1991). Since the smallest cluster identified with the *2MASS* data contains 15 stars, each of these regions would almost certainly have been identified as a cluster if they have been included in the *2MASS* Second Incremental Release. Several star forming regions in the Orion clouds found in previous studies did not meet the cluster definition adopted here, including NGC 2023, HH34, V380 Ori, the Cohen-Kuhi group, KMS 35, KMS 36, and additional low luminosity *IRAS* sources (Lada et al. 1991; Strom, Strom, & Merrill 1993; Chen & Tokunaga 1994). These star forming regions contains between 5 and 34 stars each, which is near the limit of the smallest clusters define in this study. The total cluster membership in Orion A and Orion B would not change appreciably if these regions were formally defined as clusters in this study.

Given the high extinction that is generally associated with star forming regions, deeply embedded, rich clusters ( $\gtrsim 100$  stars) could exist that remain undetected at near-infrared wavelengths. Any such clusters should appear in the *IRAS*  $60\mu\text{m}$  image which can probe deeper into molecular clouds than  $K_s$  observations. In Perseus, the brightest *IRAS* sources besides IC 348 and NGC 1333 are associated with L 1448, L 1455, and a ring of bright far-infrared emission southwest of IC 348 that is possibly related to a H II region (Andersson et al. 2000). The luminosities of these *IRAS* point sources are  $\lesssim 20 L_\odot$  (Ladd, Lada, & Myers 1993), which is too low to contain a significant cluster of young stars unless the stellar masses are strongly biased toward low mass objects. In Orion A and Orion B, each of the bright far-infrared emitting regions corresponds to a stellar cluster and therefore it is unlikely that a rich cluster remains unidentified in these clouds. In MonR2, three bright *IRAS* sources, corresponding to reflection nebula VDB 70, VDB 72 (NGC 2182), and VDB 74 (van den Bergh 1966), have no apparent clusters in the *2MASS* data. The relatively blue stellar colors and the weak  $^{13}\text{CO}$  emission indicate that the molecular gas associated with these nebula is diffuse and cannot contain a deeply embedded cluster. Two additional bright *IRAS* sources (06124-0621 and 06128-0624) are present in the northeast corner of the MonR2 molecular cloud that are coincident with moderately bright  $^{13}\text{CO}$  emission. Part of the *2MASS* point source

data in this region has been masked due to a neighboring bright star. Visual inspection of the *2MASS* Image Atlas suggests that *IRAS* 06128-0624 may be associated with a cluster of  $\approx 20$  stars, but the low far-infrared luminosity of both sources ( $\lesssim 30 L_\odot$ ) suggests that neither *IRAS* source is associated with a rich cluster. Therefore, it seems likely that the richest clusters in each of these molecular clouds have been identified from *2MASS* and published observations.

In summary, the total number of cluster members identified in the *2MASS* data after field star subtraction is  $>299$ ,  $>1992$ , 246, and 543 for Perseus, Orion A, Orion B, and MonR2, respectively. If we include observations from the literature to take into account clusters not included in the *2MASS* Second Incremental Release (NGC 1333 and NGC 2071), clusters that have been only partially mapped with *2MASS* so far (NGC 2068), and clusters that have been partially masked because of neighboring bright stars (NGC 2024), the total number of stars in clusters increases to 393 for Perseus and 606 for Orion B. Corrections to the total stellar population in IC 348, L 1641 C, and the ONC due to masked out regions are not accurately known and have not been applied. The number of clusters ranges from 2 in Perseus to 7 in Orion A, and at least half of the cluster stellar population in each cloud can be attributed to a single cluster. The fraction of the molecular cloud surface area as defined by  $^{13}\text{CO}(1-0)$  emission occupied by the clusters (including the cluster properties incorporated from the literature) is  $\approx 3\%$ , 12%, 7%, 3% in Perseus, Orion A, Orion B, and MonR2 respectively.

### 3.4. Distributed Stellar Populations

Stars associated with the molecular cloud but located outside the boundaries of the stellar clusters are defined as the distributed stellar population. The distributed population may include stars that formed in isolation, stars that formed in clusters in the past but have since dispersed into the molecular cloud, small groups of stars not meeting the adopted surface density requirements to be identified as clusters, and stars that are associated with identified clusters but lie beyond the adopted cluster boundary. The angular extent of the distributed population is unknown, so it is assumed that the stars may be located anywhere where  $^{13}\text{CO}(1-0)$  emission is detected as shown in Figures 4-7.

The signature of a distributed population is a positive average stellar surface density toward lines of sight outside the cluster boundaries but within the molecular cloud after subtracting the field star contribution to the observed star counts. Histograms of the field star subtracted,  $J$ ,  $H$ , and  $K_s$  stellar surface densities toward the Perseus, Orion A, Orion B, and MonR2 molecular clouds are shown in Figures 10-13 for the nominal extinction model. The open histograms are for all lines of sight toward the molecular clouds, and the hatched histograms are for lines of sight within the cloud that do not intercept a cluster. Each of the histograms are similar in that they peak at a surface density of  $\approx 0 \text{ arcmin}^{-2}$  with a tail toward higher values. The high surface density tails in the histograms are generally associated with clusters, although the  $J$  and  $H$  histograms for Orion A do contain a few lines of sight with high surface densities ( $> 1 \text{ arcmin}^{-2}$ ) that have been assigned

to the distributed population. These lines of sight are regions around bright stars in the ONC that were masked out at  $K_s$  band where the cluster area was defined, but not at  $J$  and  $H$  bands where a smaller region was masked out. For each cloud, the histograms extend to negative surface densities. Negative surface densities for individual pixels are expected since Poisson fluctuations in the star counts implies that the number of field stars will be less than the expected average field star surface density for some lines of sight, and exceed the field star model for others. The number of lines of sight with a negative surface density and the width of the histograms in Figures 10-13 depend on the kernel size used to generate the surface density maps and the surface density of the field star population. Since the nominal kernel width is set to a constant linear size of 0.25 pc, the angular size of the kernel will be smallest for the more distant cloud, MonR2, and largest for the nearest cloud, Perseus. The Perseus star count map will then be more heavily smoothed and have smaller fluctuations in the observed star counts about the model field star population than MonR2, as observed.

The mean surface density of the distributed population was obtained by averaging the field star subtracted surface density map for regions outside the cluster boundaries but within the  $^{13}\text{CO}$  map area as represented graphically by the hatched histograms in Figures 10-13. These mean surface densities are summarized in Table 3 for each band and the three extinction models. The formal  $1\sigma$  uncertainties in the mean stellar surface densities computed from the distribution of points in the hatched histogram are  $\approx 0.005 \text{ arcmin}^{-2}$  in each band for Perseus, Orion A, and Orion B, and  $\approx 0.009 \text{ arcmin}^{-2}$  for MonR2. By comparison, the range in the surface densities due to the uncertainties in the extinction model are  $\approx \pm 0.10$ , 0.05, and  $0.03 \text{ arcmin}^{-2}$  at  $J$ ,  $H$ , and  $K_s$  respectively (see Table 3). As mentioned in Section 3.1, however, the uncertainties due to the extinction model are not formal  $1\sigma$  confidence intervals but represent the plausible range of values based upon converting the  $^{13}\text{CO}$  integrated intensity into visual extinction. Thus compared to the other field star model uncertainties discussed in Section 3.1, the largest source of uncertainty in the mean stellar surface density for the distributed population is converting the  $^{13}\text{CO}$  integrated intensity to visual extinction.

The range of possible surface densities for the distributed population from the three extinction models is shown graphically in Figures 14-17. These figures show the field star subtracted surface density averaged over Galactic latitude for each cloud as a function of Galactic longitude for the nominal extinction model. The surface density of the distributed population for the nominal extinction model is shown by the solid horizontal line, and the dashed lines show the corresponding surface densities derived from the low and high extinction models. The top panel in each figure shows the average visual extinction also averaged over Galactic latitude. The narrow peaks in the surface density at discrete Galactic latitudes represent the compact stellar clusters, although the large angular extent of the Orion Nebula Cluster is clearly visible. Figures 14-17 indicate that within a given cloud, the  $J$ ,  $H$ , and  $K_s$  data give a consistent value for the distributed population surface density within the uncertainties of the field star subtraction. The most stringent constraints on the distributed population is provided at  $K_s$  band, which is the least sensitive of

the three bands to the assumed extinction model. Therefore, the characteristics of the distributed population discussed below will be based primarily on the  $K_s$  band data. Table 3 indicates that for the nominal extinction model, the Perseus, Orion A, and MonR2 molecular clouds contain a positive mean stellar surface density that is indicative of a distributed population, while Orion B has a negative surface density. For the low extinction model, the Perseus molecular cloud has also a negative implied surface density for the distribution population. A negative mean surface density for the distributed population is unphysical and indicates that too many field stars were subtracted from the observed star counts for that particular extinction model. The number of stars contained in the distributed population over the entire cloud as mapped in  $^{13}\text{CO}$  was computed by multiplying the average surface density by the cloud area (see Table 1), including those regions not encompassed by the *2MASS* Second Incremental Release. The magnitude of the distributed population inferred from the  $K_s$  band observations ranges from zero stars in Orion B to  $\approx 730$  in Orion A. However, given the uncertainty in the extinction, a distributed population consisting of  $\approx 790$  stars cannot be ruled out even in Orion B. These estimates for the number of stars in the distributed population refer only to stars that fall within the adopted magnitude thresholds. The fraction of the distributed stellar population that may exist but have magnitudes outside these thresholds is considered in Section 4.1.

The surface density of the distributed population can be compared with previous observations of the Orion A and Orion B molecular clouds. Lada et al. (1991) found that the surface density for the distributed population in Orion B of  $\approx 0.007 \text{ arcmin}^{-2}$  for stars with  $K < 13^m$  over a  $0.7 \text{ deg}^2$  region. Li, Evans, & Lada (1997) observed a  $0.37 \text{ deg}^2$  region away from known clusters at  $J$ ,  $H$ , and  $K$  band in Orion B, and inferred that the surface density of stars in the distributed population with a near-infrared excess in the  $J - H$  vs.  $H - K$  color-color diagram is  $< 0.014 \text{ arcmin}^{-2}$ . Both of these results are consistent with values obtained here for Orion B within the uncertainties of the field star subtraction. Strom, Strom, & Merrill (1993) analyzed the stellar population in Orion A based on a near-infrared imaging survey encompassing a total of  $0.77 \text{ deg}^2$  of the cloud area. In addition to identifying several clusters, they measured a distributed population of  $\approx 1500$  stars down to a  $5\sigma$  detection limit of  $J = 16.8^m$ , implying a surface density for the distributed population of  $\approx 0.54 \text{ stars arcmin}^{-2}$ . By comparison, the maximum surface density for the distributed population in Orion A implied by the *2MASS* data is  $0.099 \text{ stars arcmin}^{-2}$ . The discrepancy between the Strom, Strom, & Merrill (1993) results and those obtained here are unclear. While Strom, Strom, & Merrill (1993) analyzed their data at a  $J$  band magnitude limit  $0.7^m$  fainter than adopted here, Figures 9 and 11 in that paper suggests that most of the distributed population they found should have  $J$  band magnitudes brighter than  $16^m$  and be detectable with the magnitudes limits adopted here. Given that the *2MASS*  $J$ ,  $H$ , and  $K_s$  star counts analyzed here are based on more extensive observations and provide consistent results, we will use these data to characterize the distributed population in Orion A.

#### 4. Implications for Global Star Formation Properties of Molecular Clouds

A complete picture of the star formation history of molecular clouds requires extensive spectroscopic and photometric observations of the cluster and distributed populations. Constraints on the star formation history of molecular clouds can be obtained though by using the star count results from the previous section and examining the relative contribution of clusters and distributed populations to the total stellar population. The ages of several clusters in nearby molecular clouds have been inferred by constructing HR diagrams and comparing the stellar effective temperatures and luminosities with pre-main-sequence evolutionary tracks, including  $\rho$  Ophiuchus (Greene & Meyer 1995; Luhman & Rieke 1999), IC 348 (Luhman et al. 1998; Herbig 1998), the Orion Nebula Cluster (Hillenbrand 1997), NGC 2024 (Meyer 1996), L1641 N (Hodapp & Deane 1993; Allen 1996), and L1641 South (Allen 1996). A literal interpretation of the HR diagrams indicate that most of the stars in these clusters have formed within the last 1-2 Myr, although some stars may be as old as 10 Myr. By comparison,  $^{12}\text{CO}$  observations of OB associations (Bash, Green, & Peters 1977; Leisawitz 1990) and the observed fraction of molecular clouds with current star formation suggest that the cloud lifetime is between 10 Myr and 100 Myr (Elmegreen 1991). Even longer lifetimes though are required in coagulation models for cloud formation (Kwan & Valdes 1983). Relative to the expected lifetime of molecular clouds then, embedded clusters represent a recent “burst” of star formation. A distributed stellar population cannot be interpreted unambiguously, as it can represent either older clusters that have since dispersed or stars of all ages that formed in isolation throughout the cloud. The relative number of the total stellar population (cluster plus distributed) currently contained in clusters then places a lower limit on the fraction of stars that have formed in the recent history of a molecular cloud.

##### 4.1. Sensitivity

Before examining the implications of the star count results for the star formation history of the molecular clouds studied here, it is important to recognize the sensitivity of the *2MASS* observations to stars of various masses and ages. These dependencies are examined in Figure 18, which shows  $K_s$  band iso-magnitude curves for stars as a function of stellar age ( $10^5 - 10^8$  years) and stellar mass ( $0.08 - 3.0 M_\odot$ ) at the distance of Perseus, Orion A/B, and MonR2. The magnitudes were computed using the pre-main-sequence evolutionary tracks from D’Antona & Mazzitelli (1997,98) assuming zero extinction and no near-infrared excess as outlined in Hillenbrand & Carpenter (2000). Only the  $K_s$  band sensitivity limits are considered here since, as shown in Section 3.4, the  $K_s$  band star counts provide the tightest constraint on the surface density of the distribution population. Figure 18 shows, for example, that at the distance of the Perseus molecular cloud,  $0.08 M_\odot$  stars are brighter than the adopted  $K_s$  band magnitude threshold for ages  $\lesssim 10$  Myr. (Young brown dwarfs with masses  $< 0.08 M_\odot$ , if present, are also detected at these distances for young ages. The shape of the initial mass function for these objects remains uncertain at this time, however, and these low masses are not considered here.) At older ages, low mass pre-main-sequence stars become

systematically fainter than the sensitivity limits of the survey and would no longer be detectable. Assuming that clouds have ages  $\lesssim 100$  Myr, Figure 18 shows that all stars more massive than  $\approx 0.3 M_{\odot}$  on the surface of the Perseus molecular clouds will be detectable, with corresponding limits of  $\approx 0.5 M_{\odot}$  for Orion A and Orion B and  $\approx 0.7 M_{\odot}$  for MonR2.

The fraction of the total stellar population that is detectable with *2MASS* depends on the mass and age distribution of the constituent stars. These distributions are crudely known for only a handful of clusters and are completely unknown for the distributed population. Therefore, we have assumed that the stars have been forming at a constant rate in time throughout the cloud with a Miller-Scalo Initial Mass Function (Miller & Scalo 1979) between 0.08 and  $10 M_{\odot}$ . The magnitudes for this model stellar population were calculated using the pre-main-sequence tracks up to  $3 M_{\odot}$  as described above. Stars more massive than  $3 M_{\odot}$  are not included in the D'Antona & Mazzitelli (1997) models, but since their pre-main-sequence phase lasts for only  $\lesssim 2$  Myr (Palla & Stahler 1993), the magnitudes of these stars as they appear on the zero age main sequence were adopted for all ages. The average visual extinction computed from the  $^{13}\text{CO}$  maps ( $3.0^m$ ,  $3.2^m$ , and  $2.6^m$  for Perseus, Orion A/B, and MonR2 respectively) were applied to the computed magnitudes.

Figure 19 shows the fraction of the model stellar population that has apparent  $K_s$  magnitudes between  $6.0^m$  and  $14.3^m$  as a function of the time. While the model is intended mainly to describe a distributed population forming over an extended period of time, the results can be applied to clusters as well. This figure indicates that for clusters, which have typical ages  $\lesssim 2$  Myr as discussed above,  $\gtrsim 80\%$  of the cluster members with stellar masses  $\geq 0.08 M_{\odot}$  are detectable with *2MASS* for each of the molecular clouds studied here. (Note, however, that clusters often have high extinction assumed for this model.) On the other hand, for a distributed population that has been forming stars for 50 Myr, 67% of the stars would be detectable in Perseus, 45% in Orion A and Orion B, and only 26% in MonR2. This model demonstrates that if the distributed population has been forming for over tens of million of years, an appreciable fraction of the stars would no longer be detectable within the adopted magnitude thresholds.

#### 4.2. Star Formation Efficiency

Given the above calculations, the observed surface density can be used to place constraints on the time averaged star formation efficiency in molecular clouds, where the star formation efficiency is defined as the fraction of the cloud mass that has been converted into stars. The predicted surface density of stars can be computed using the cloud masses and angular areas summarized in Table 1, and assuming that the stars have been forming at a constant rate in time with a Miller-Scalo Initial Mass Function between  $0.08 M_{\odot}$  and  $10 M_{\odot}$ . The solid curves in Figure 20 show the predicted  $K_s$  surface density for stars with magnitudes of  $6.0^m \leq m(K_s) \leq 14.3^m$  for the nominal extinction model assuming star formation efficiencies of 1%, 2%, 5%, and 8%. The dashed lines in Figure 20 show the observed stellar surface density for the distributed population only. Similarly, the dotted lines show the surface density of the clusters only, averaged over the entire cloud area

in order to determine how efficient mass is being converted into clusters on a global scale. The star formation efficiencies in the dense cores that the clusters formed in will naturally be higher. As with Figure 19, the older ages are intended to apply only to the distributed population and not the clusters. Figure 20 indicates that the star formation efficiency implied by the distributed population alone is <1% for Perseus, 1-5% for Orion A, 0% for Orion B, and 1-4% for MonR2, where the range is due to the uncertain ages of the distributed population. The star formation efficiency implied by the clusters only is  $\approx$ 2% in Perseus, 4% in Orion A, 1% in Orion B, and 1% in MonR2. The total star formation efficiency implied by the sum of the cluster and distribution populations then ranges from a low of  $\approx$ 1% in Orion B to a high of 9% in Orion A if the distribution population is as old as 100 Myr.

### 4.3. The Fraction of Stars in Clusters

Since the observed ages of clusters is  $\lesssim$ 2 Myr, the fraction of the total stellar population contained in clusters alone reflects the relative contributions of recent star formation activity compared to isolated star forming regions and older stars that constitute the distributed population. The fraction of the detected stellar population contained in clusters using the nominal extinction model is 80%, 73%, 100%, and 56% for Perseus, Orion A, Orion B, and MonR2 respectively, where the contributions to the stellar population from previously known clusters not contained in the 2MASS Second Incremental Release have been included (see Section 3.3). The cluster fraction may be as high as 100%, 87%, 100%, and 74% for these clouds if the low extinction model is adopted, and as low as 34%, 59%, 39%, and 41% with the high extinction model. As emphasized above, however, an appreciable fraction of the distributed population may not have been detected if the stellar population has been forming for more than several million years. Thus the observed fraction of stars in clusters may underestimate the contribution from the distributed population. The number of stars in the distributed population that are too faint to detect with the present observations was estimated in Figure 19 assuming a constant star formation rate and a Miller-Scalo IMF. Applying these assumptions and model calculations, Figure 21 shows the implied fraction of the total stellar population contained in clusters as a function of age for the distributed population. The solid curve shows the fraction of stars in clusters for the nominal extinction model, and the dotted curves represent the cluster fraction for the low and high extinction models. After taking into account the ages of the distributed population, the fraction of stars contained in clusters under the nominal extinction model is  $\gtrsim$ 50% in Perseus, Orion A, and Orion B for ages less than 100 Myr, and  $\gtrsim$ 25% for MonR2. Even for the high extinction model and an old age (100 Myr), the fraction of stars in clusters is still between 17-41% for the four clouds. Thus in each of these molecular clouds, a substantial fraction of the total stellar population, if not the majority, is contained in young stellar clusters.

#### 4.4. Discussion

The substantial fraction of stars found in clusters regardless of the age of the distributed population is surprising given the canonical assumed lifetimes of molecular clouds. As discussed above, embedded, dense clusters typically have ages  $\lesssim 2$  Myr. The fact that no substantially older clusters are found within molecular clouds indicates that these older clusters have dispersed into the molecular cloud, have destroyed the surrounding molecular gas and no longer appear associated with a cloud, or these clouds are just now forming their first clusters. If we assume a constant star formation rate and that clusters simply disperse after a few million years, then the fraction of stars contained in clusters should decrease as  $t^{-1}$ , where  $t$  is the age of the molecular cloud. With these assumptions and assuming a cloud lifetime of 50 Myr just as an example, the fraction of stars in clusters should be  $\approx 4\%$ . By contrast, the observed fraction of stars in clusters for the clouds analyzed here is substantially higher as discussed above, and would imply a cloud lifetime of  $\lesssim 7$  Myr under the constant star formation rate assumption even given the uncertainties in the field star subtraction. Thus in each of the clouds, the distributed population contains fewer stars than expected if star formation has been occurring in these regions at a constant rate for tens of millions of years. This situation is reminiscent of the post-T Tauri star problem in the Taurus molecular cloud, where most stars within the confines of the molecular gas have ages  $\lesssim 3$  Myr and few stars have been identified that are older than 10 Myr (Herbig 1978). Various hypotheses have been proposed to explain the lack of older stars in Taurus and other nearby molecular clouds, including the kinematic dispersal of older stars from the molecular cloud boundaries, imposing a star formation rate that changes with time, and postulating that molecular clouds are inherently short lived. We briefly discuss these possibilities as they pertain to the Perseus, Orion A, Orion B, and MonR2 molecular clouds.

The small number of old stars that have been identified in nearby molecular clouds has led to the suggestion that a substantial fraction of the stellar population has dispersed from the molecular gas and that the current stellar census is incomplete (Feigelson 1996). Assuming a one dimensional velocity of  $1 \text{ km s}^{-1}$ , a star could drift as far as 10 pc ( $1.2^\circ$  at the distance of Orion A and Orion B) in 10 Myr. However, molecular clouds are likely gravitationally bound structures, and presumably the kinematics of the newly formed stars reflect that of the molecular gas. Since the star formation efficiency implied by the star counts is  $\lesssim 9\%$ , the dynamical evolution of the embedded stars will be dominated by the gas as long as the cloud remains intact. Therefore, many, if not most, of the stars must remain within the cloud. Nevertheless, the size of any dispersed stellar population can be gauged from H $\alpha$  and X-ray surveys of regions surrounding the cloud. This has been in fact done for the Orion A and Orion B molecular clouds, but the results remain inconclusive. Both H $\alpha$  (Nakano, Wiramihardja, & Kogure 1995) and X-ray (Sterzik et al. 1995) surveys of this region find a source density of  $\approx 1 \text{ star deg}^{-2}$  in regions surrounding the Orion molecular clouds and OB association. Up to one-third of the X-ray sources may be unrelated foreground stars (Alcalá et al. 2000, 1996; Alcalá, Chavarriá-K., & Terranegra 1998) perhaps related to Gould's belt (Guillout et al. 1998), but in any event, the surface density of sources is too low to contribute significantly to the total

population in the Orion A and Orion B molecular clouds relative to the clusters.  $\text{H}\alpha$  emission is likely not sensitive to the majority of the older stars likely to constitute a old dispersed population, though, and at the distance of the Orion clouds, the ROSAT All Sky Survey is able to detect only to the more luminous X-ray T Tauri stars (Neuhäuser et al. 1995; Alcalá et al. 2000). In more nearby clouds, however, follow up studies of the widely distributed ROSAT X-ray sources indicate that many these objects likely do not represent a dispersed population, but rather solar-type zero age main sequence stars or older pre-main-sequence stars unrelated to the existing molecular clouds (Magazzù et al. 1997; see also Briceño et al. 1997, Favata, Micela, & Sciortino 1997). Further, a large scale X-ray and objective-prism survey of Taurus failed to find any new T Tauri stars older than 5 Myr (Briceño et al. 1999).

If most of the stars that have formed over the lifetime of the Perseus, Orion A, Orion B, and MonR2 molecular clouds are still associated with the molecular gas, then the high fraction of the total stellar population contained in clusters implies that either the star formation rate is currently higher than it has been in the past (Palla & Galli 1997; Palla & Stahler 2000), or that molecular clouds have relatively young ages (Ballesteros-Paredes, Hartmann, & Vázquez-Semadeni 1999; Elmegreen 2000). Palla & Stahler (2000) re-analyzed published HR diagrams for a number of nearby star forming regions with a single set of pre-main-sequence models and argued that star formation over entire molecular clouds (e.g. Taurus and Chamaeleon I) and individual clusters (e.g. the Orion Nebula Cluster) started at a low rate  $\gtrsim 10$  Myr ago and has increased dramatically within the past 1-3 Myr. In their scenario, molecular clouds remain relatively dormant for much of their cloud lifetime since individual dense cores are supported against gravitational collapse by magnetic fields, and the time scale to dissipate the magnetic support is on the order of  $\approx 10$  Myr (see also Palla & Galli 1997). Ballesteros-Paredes, Hartmann, & Vázquez-Semadeni (1999), on the other hand, suggested that the lack of old stars in Taurus this is a consequence of the molecular filaments that make up the cloud having formed only within the past few million years in turbulent flows in the interstellar medium. In this scenario, Taurus is an intrinsically young cloud that has not had time to form old stars (see also Elmegreen 2000).

The difference between the two pictures for the evolution of molecular clouds has important consequences for molecular cloud evolution. In the Palla & Galli (1997) scenario, molecular clouds are in a quasi-static state for most of their lifetime, while the Ballesteros-Paredes, Hartmann, & Vázquez-Semadeni (1999) model suggest clouds form and evolve dynamically in the interstellar medium. If the Palla & Stahler (2000) model is correct, most molecular clouds should not contain a substantial stellar population since they are relatively dormant for most of their cloud lifetimes. The difficulty with this scenario is that it would imply that we are observing a number of molecular clouds in the solar neighborhood just as they are forming a substantial fraction of their total stellar population in young clusters. This would include not only the 4 molecular clouds studied here, but also Chamaeleon I, Lupus, and Taurus. This is not necessarily an observational bias in that these clouds are frequently studied because they have active star formation, as star formation and stellar clusters appear to be ubiquitous in molecular clouds. More than half of the clouds within 200 pc of

the sun are forming an appreciable number of T Tauri stars (Feigelson 1996 and references therein), and most Giant Molecular Clouds within 3 kpc of the sun are forming OB stars and presumably an accompanied clusters of lower mass stars (Blitz 1991). In this respect, imposing a short lifetime for molecular clouds would qualitatively account for the lack of a substantial older stellar population in molecular clouds without the need to impose a higher than average star formation rate at the current time (Ballesteros-Paredes, Hartmann, & Vázquez-Semadeni 1999; Elmegreen 2000). A more systematic survey of a volume limited sample of molecular clouds seems warranted though to better establish the frequency of clusters within molecular clouds as a more comprehensive observational test of these two pictures of cloud evolution.

## 5. Summary

We investigate the spatial distribution of young stars associated with the Perseus, Orion A, Orion B, and MonR2 molecular clouds using  $J$ ,  $H$ , and  $K_s$  star counts from the *2MASS* Second Incremental Release. The stellar population associated within these clouds is determined statistically by subtracting a semi-empirical model for the field star contamination from the observed stellar surface density maps. The field star model is constructed using *2MASS* observations of the regions surrounding the clouds to measure the total field star surface density, published  $^{13}\text{CO}(1-0)$  maps to determine the cloud extinction, and the Wainscoat et al. (1992) Galactic star count model to estimate the fraction of field stars that are background to the clouds. The stellar population is categorized into compact stellar clusters and a distributed stellar population. Individual stellar clusters are identified as peaks in the field star subtracted, stellar surface density maps, and the distributed stellar population is defined as any excess star counts outside the cluster boundaries but within the molecular cloud as traced by  $^{13}\text{CO}(1-0)$  emission.

The number of clusters within the studied molecular clouds, including clusters identified in the literature in regions not yet observed with *2MASS*, varies from 2 in Perseus to 7 in Orion A. The total number of stars contained within the clusters is  $>393$  in Perseus,  $>1992$  in Orion A, 606 in Orion B, and 543 in MonR2. More than half of the cluster members in each cloud is contained in just a single rich cluster. A distributed stellar population is detected in the Orion A and MonR2 molecular clouds within the uncertainties of the fieldstar subtraction at a  $K_s$  band surface density between  $0.013 \text{ arcmin}^{-2}$  and  $0.084 \text{ arcmin}^{-2}$ . Model calculations suggest, however, that the surface density of the distributed population in the clouds may be underestimated by as much as a factor of three if the stars have been forming with a Miller-Scalo Initial Mass Function between  $0.08 M_{\odot}$  and  $10 M_{\odot}$  at a constant star formation rate for up to 100 Myr. After taking into consideration the possible evolutionary status of the distributed population, the star formation efficiencies implied by the sum of cluster and distributed populations varies between  $\approx 1\text{-}9\%$  for the four clouds. The percentage of the total observed stellar population contained in clusters alone is 80%, 73%, 100%, and 56% for Perseus, Orion A, Orion B, and MonR2 respectively for the nominal extinction model, but may be up to a factor of two lower depending again on the age of

the distributed population. Nonetheless, the high fraction of stars currently contained in clusters is surprising given that embedded clusters typically have ages ( $\lesssim 2$  Myr) that are substantially younger than that often assumed for molecular clouds (10-100 Myr). These results indicate that either each of these molecular clouds have been forming stars at a higher rate in the last couple of million years than in the prior history, or that the ages of molecular clouds are younger than generally assumed.

JMC would like to thank Lynne Hillenbrand for numerous discussions and comments on this work. He is also grateful to John Bally for providing the  $^{13}\text{CO}$  molecular line maps. This publication makes use of data products from the Two Micron All Sky Survey, which is a joint project of the University of Massachusetts and the Infrared Processing and Analysis Center, funded by the National Aeronautics and Space Administration and the National Science Foundation. JMC acknowledges support Long Term Space Astrophysics Grant NAG5-8217 and the Owens Valley Radio Observatory, which is supported by the National Science Foundation through NSF grant AST 9981546.

## REFERENCES

Alcalá, J. M., Chavarriá-K. C., & Terranegra, L. 1998, A&A, 330, 1017

Alcalá, J. M., Covino, E., Torres, G., Sterzik, M. F., Pfeiffer, M. J., & Neuhäuser, R. 2000, A&A, 353, 186

Alcalá, J. M., Terranegra, L., Wichmann, R., Chavarriá-K. C., Krautter, J., Schmitt, J. H. M. M., Moreno-Corral, M. A., de Lara, E., & Wagner, R. M. 1996, A&AS, 119, 7

Ali, B., & Depoy, D. L. 1995, AJ, 109, 709

Allen, L. E. 1996, Ph.D. Thesis, University of Massachusetts

Allen, L. E., & Hillenbrand, L. A. 2000, to appear in “Proceedings of the Ringberg Castle Conference on Orion”, PASP Conference proceedings, ed. M. McCaughrean, in press

Andersson, B-G, Wannier, P. G., Moriarty-Schieven, G. H., & Bakker, E. J. 2000, ApJ, 119, 1325

Aspin, C., & Sandell, G., 1997, MNRAS, 289, 1

Aspin, C., Sandell, G., & Russell, A. P. G. 1994, A&AS, 106, 165

Aspin, C., & Walther, D. M. 1990, A&A, 235, 387

Bachiller, R., & Cernicharo, J. 1986, A&A, 166, 283

Ballesteros-Paredes, J., Hartmann, L., & Vázquez-Semadeni, E. 1999, ApJ, 527, 285

Bally, J., Stark, A. A., Wilson, R. W., & Langer, W. D. 1987, ApJ, 312, L45

Barsony, M., Kenyon, S. J., Lada, E. A., & Teuben, P. J. 1997, ApJS, 112, 109

Bash, F. N., Green, E., & Peters, W. L. III 1977, ApJ, 217, 464

Beichman, C. A., Myers, P. C., Emerson, J. P., Harris, S., Mathieu, P., Benson, P. J., & Jennings, R. E. 1986, ApJ, 307, 337

Bessell, M. S., & Brett, J. M. 1988, PASP, 100, 1134

Blitz, L. 1991, in *The Physics of Star Formation*, eds. C. J. Lada & N. Kylafis, (Dordrecht:Kluwer), 3

Briceño, C., Calvet, N., Kenyon, S., & Hartmann, L. 1999, ApJ, 118, 1354

Briceño, C., Hartmann, L. W., Stauffer, J. R., Gagné, M., Stern, R., & Caillault, J-P. 1997, AJ, 113, 740

Brown, A. G. A., de Geus, E. J., & de Zeeuw, P. T. 1994, A&A, 289, 101

Cambrésy, L. 1999, A&A, 345, 965

Cambrésy, L., Copet, E., Epcstein, N., de Batz, B., Borsenberger, J., Fouqué, Kimeswenger, S., Tiphène, D. 1998, A&A, 338, 977

Carpenter, J. M., Meyer, M. R., Dougados, C., Strom, S. E., & Hillenbrand, L. A. 1997, AJ, 114, 198

Chen, H., & Tokunaga, A. T. 1994, ApJS, 90, 149

Chen, H., Tokunaga, A. T., Strom, K. M., & Hodapp, K. W. 1993, ApJ, 407, 639

Clarke, C. J., Bonnell, I. A., & Hillenbrand, L. A. 2000, in Protostars and Planets IV, ed. V. Mannings, A. P. Boss, and S. S. Russell (Tucson: University of Arizona Press), in press

Cohen, J. G., Grogel, J. A., Perrson, S. E., & Elias, J. H. 1981, ApJ, 249, 481

Comerón, F., Rieke, G. H., & Rieke, M. J. 1996, ApJ, 473, 294

Dame, T. M., Ungerechts, H., Cohen, R. S., de Geus, E. J., Grenier, I. A., May, J., Murphy, D. C., Nyman, L.-A., & Thaddeus, P. 1987, ApJ, 322, 706

D'Antona, F. & Mazzitelli, I. 1997, MmSAI 68, 807

\_\_\_\_\_. 1998, private communication

de Zeeuw, P. T., Hoogerwerf, R., de Bruijne, J. H. J., Brown, A. G. A., & Blaauw, A. 1999, ApJS, 117, 354

Elmegreen, B. G. 1991, in *The Physics of Star Formation*, eds. C. J. Lada & N. Kylafis, (Dordrecht:Kluwer), 35

\_\_\_\_\_. 2000, ApJ, 530, 277

Favata, F., Micela, G., & Sciortino, S. 1997, A&A, 326, 647

Feigelson, E. D. 1996, ApJ, 468, 306

Frerking, M. A., Langer, W. D., & Wilson, R. W. 1982, ApJ, 262, 590

Genzel, R., Reid, M.J., Moran, J.M., & Downes, D. 1981, ApJ 224, 884

Gomez, M., Hartmann, L., Kenyon, S. J., & Hewett, R. 1994, AJ, 105, 1927

Greene, T. P., & Meyer, M. R. 1995, ApJ, 450, 233

Guillout, P., Sterzik, M. F., Schmitt, J. H. M. M., Motch, C., & Neuhäuser, R. 1998, A&A, 337, 113

Gyulbudaghian, A. L., Glushkov, Yu. I., & Denisyuk, E. K. 1978, *ApJ*, 224, L137

Hayakawa, T., Mizuno, A., Onishi, T., Yonekura, Y., Hara, A., Yamaguchi, R., & Fukui, Y. 1999, *PASP*, 51, 919

Herbig, G. H. 1978, in *Problems of Physics and Evolution of the Universe*, ed. L. Mirzoyan (Yerevan: Acad. Sci. Armenian S. S. R.), 171

Herbig, G. H. 1998, *ApJ*, 497, 736

Herbst, W., & Racine, R. 1976, *AJ*, 81, 840

Hillenbrand, L. A. 1997, *AJ*, 113, 1733

Hillenbrand, L.A., & Carpenter, J. M. 2000, *ApJ*, 540, 236

Hillenbrand, L.A., & Hartmann, L. W. 1998, *ApJ*, 492, 540

Hodapp, K. W., & Deane, J. 1993, *ApJS*, 88, 119

Howard, E. M., Pipher, J. L., & Forrest, W. J. 1994, *ApJ*, 425, 707

Johnstone, D., & Bally, J. 1999, *ApJ*, 510, L49

Jones, B. F., & Walker, M. F. 1988, *AJ*, 95, 1755

Kwan, J., & Valdes, F. 1983, *ApJ*, 271, 604

Lada, C. J., Alves, J., & Lada, E. A. 1996, *AJ*, 111, 1964

Lada, C. J., Lada, E. A., Clemens, D. P., & Bally, J. 1994, *ApJ*, 429, 694

Lada, C. J., Young, E. T., & Greene, T. P. 1993, *ApJ*, 408, 471

Lada, E. A., DePoy, D. L., Evans, N. J. II, & Gatley, I. 1991, *ApJ*, 371, 171

Lada, E. A., & Lada, C. J. 1995, *AJ*, 109, 1682

Ladd, E. F., Lada, E. A., & Myers, P. C. 1993, *ApJ*, 410, 168

Langer, W. D., Wilson, R. W., Goldsmith, P. F., & Beichman, C. A. 1989, *ApJ*, 337, 355

Lee, Y., Snell, R. L., & Dickman, R. L. 1994, *ApJ*, 432, 167

Leisawitz, D. 1990, *ApJ*, 359, 319

Li, W., Evans, N. J. II, & Lada, E. A. 1997, *ApJ*, 488, 277

Lis, D. C., Serabyn, E., Keene, J., Dowell, C. D., Benford, D. J., Phillips, T. G., Hunter, T. R., & Wang, N. 1998, *ApJ*, 509, 299

Luhman, K. L. 1999, *ApJ*, 525, 466

Luhman, K. L., & Rieke, G. H. 1999, *ApJ*, 525, 440

Luhman, K. L., Rieke, G. H., Lada, C. J., & Lada, E. A. 1998, *ApJ*, 508, 347

Maddalena, R. J., Moscowitz, J., Thaddeus, P., & Morris, M. 1986, *ApJ*, 303, 375

Magazzù, A., Martín, E. L., Sterzik, M. F., Neuhäuser, R., Covino, E., & Alcalá, J. M. 1997, *A&AS*, 124, 449

McCaughrean, M. J., & Stauffer, J. R. 1994, *AJ*, 108, 1382

Meyer, M. R. 1996, Ph.D. Thesis, University of Massachusetts

Meyer, M. R., & Lada, E. A. 2000, to appear in “Proceedings of the Ringberg Castle Conference on Orion”, *PASP* Conference proceedings, ed. M. McCaughrean, in press

Miesch, M. S., & Bally, J. 1994, *ApJ*, 429, 645

Miller, G. E., & Scalo, J. M. 1979, *ApJS*, 41, 513

Nagahama, T., Mizuno, A., Ogawa, H., & Fukui, Y. 1998, *AJ*, 116, 336

Nakono, M., Wiramihardja, S.D., & Kogure, T. 1995, *PASJ*, 47, 889

Neuhäuser, R., Sterzik, M. F., Schmitt, J. H. M. M., Wichmann, R., & Krautter, J. 1995, *A&A*, 297, 391

Padoan, P., Bally, J., Billawala, Y., Juvela, M., & Nordlund, A. 1999, *ApJ*, 525, 318

Palla, F., & Galli, F. 1997, *ApJ*, 476, L35

Palla, F., & Stahler, S. W. 1993, *ApJ*, 418, 414

\_\_\_\_\_. *ApJ*, in press

Phelps, R. L., & Lada, E. A. 1997, *ApJ*, 477, 176

Piche, F. 1993, *PASP*, 105, 324

Prosser, C. F., Stauffer, J. R., Hartman, L., Soderblom, D. R., Jones, B. F., Werner, M. W., & McCaughrean, M. J. 1994, *ApJ*, 421, 517

Reach, W. T., Wall, W. F., & Odegard, N. 1998, *ApJ*, 507, 507

Silverman, B. W., 1986, *Density Estimation for Statistics and Data Analysis*, (London:Chapman & Hall)

Sterzik, M. F., Alcalá, J. M., Meuhaeuser, R., & Schmitt, J. H. M. M. 1995, *A&A*, 297, 418

Strom, K. M., Kepner, J., & Strom, S. E. 1995, *ApJ*, 438, 813

Strom, K. M., Strom, S. E., & Merrill, K. M. 1993, *ApJ*, 412, 233

Tatematsu, K., Umemoto, T., Heyer, M. H., Hirano, N., Kameya, O., & Jaffe, D. T. 1998, *ApJS*, 118, 517

van den Bergh, S. 1966, *AJ*, 71, 990

Wainscoat, R. J., Cohen, M., Volk, K., Walker, H. J., & Schwartz, D. E. 1992, *ApJS*, 83, 111

Walter, F. M., Brown, A., Mathieu, R. D., Myers, P. C., & Vrba, F. V. 1988, *AJ*, 96, 297

Fig. 1.— A  $K_s$  band stellar surface density map for point sources in the *2MASS* Second Incremental Release for the area between Galactic longitudes of  $130^\circ$  and  $250^\circ$  and Galactic latitudes of  $-40^\circ$  and  $+40^\circ$ . The map was produced by binning stars with magnitudes  $6.0^m \leq m(K_s) \leq 14.3^m$  in  $5' \times 5'$  pixels. The map is presented in the Hammer-Aitoff projection with a square-root image stretch. Darker gray scales denote higher stellar surface densities, with the surface densities ranging from  $\approx 2 \text{ arcmin}^{-2}$  in the Galactic Plane to  $\approx 0.2 \text{ arcmin}^{-2}$  at higher Galactic latitudes. The white regions represent tiles not included in the Second Incremental Release, or in less than 1% of the instances, tiles not meeting the sensitivity criteria adopted for this paper (see text). The location of several well known molecular clouds are indicated.

Fig. 2.— Image of the average  $J - K_s$  stellar color over the same region shown in Figure 1. The darker gray scales represent larger  $J - K_s$  colors and indicate regions where background field stars and embedded young stars have been reddened by dust in molecular clouds. The Taurus, Perseus, Orion A, Orion B, and MonR2 molecular clouds are clearly visible, as well as numerous molecular clouds within the Galactic Plane.

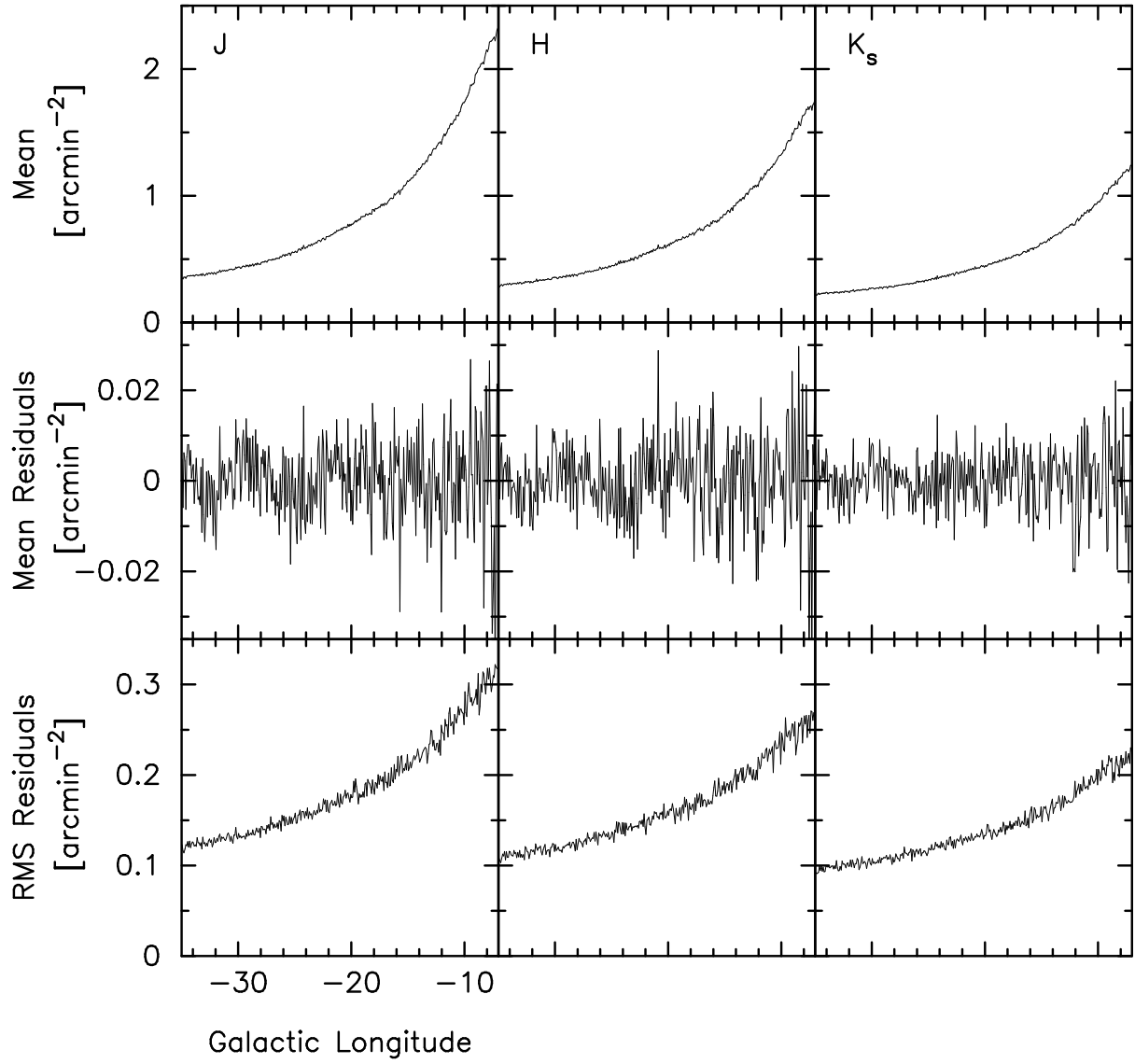


Fig. 3.— The observed mean stellar surface density as a function of Galactic latitude (top panels), the mean residuals after subtracting a polynomial fit to the observed star counts (middle panels), and the RMS of the residuals (bottom panels) at  $J$ ,  $H$ , and  $K_s$  band. Only regions between Galactic longitudes of  $130^\circ$  and  $250^\circ$  and latitudes of  $-35^\circ$  and  $-7^\circ$  that did not contain a stellar cluster or a molecular cloud are shown here and included in the polynomial fit. The fit was performed as a function of both Galactic longitude and latitude, but are averaged over longitude for presentation in this figure. For reference, the Perseus, Orion A, Orion B, and MonR2 molecular clouds analyzed in this paper are located between latitudes of  $-20^\circ$  and  $-10^\circ$ .

Fig. 4.— *Upper left*: An adaptive kernel,  $K_s$  band stellar surface density map of the Perseus molecular cloud for stars with magnitudes of  $6.0^m \leq m(K_s) \leq 14.3^m$ . *Upper right*: The *IRAS*  $60\mu\text{m}$  image displayed in a logarithmic stretch. *Lower left*: An image of the average  $J - K_s$  color for stars observed by *2MASS*. *Lower right*: A map of the integrated  $^{13}\text{CO}(1-0)$  intensity map (Padoan et al. 1999). In each panel, darker halftones represent the higher intensities. In the  $K_s$  density map and the average  $J - K_s$  color image, the white strips are tiles not included in the *2MASS* Second Incremental Release, and the white “crosses” are regions around bright stars that were masked out when generating the Second Incremental Release Point Source Catalog. The labels indicate the location of either prominent star forming regions or stellar clusters identified in the  $K_s$  surface density image (see Table 2).

Fig. 5.— Same as in Figure 4, except for the Orion A (L1641) molecular cloud. The  $^{13}\text{CO}$  image is from Bally et al. (1987).

Fig. 6.— Same as in Figure 4, except for the Orion B (L1630) molecular cloud. The  $^{13}\text{CO}$  image is from Miesch & Bally (1994).

Fig. 7.— Same as in Figure 4, except for the MonR2 molecular cloud. The  $^{13}\text{CO}$  image is from Miesch & Bally (1994). The sources labeled VDB are reflection nebula cataloged by van den Bergh (1966), and sources labeled GGD are from the list of Herbig-Haro objects noted by Gyulbudaghian, Glushkov, & Denisyuk (1978).

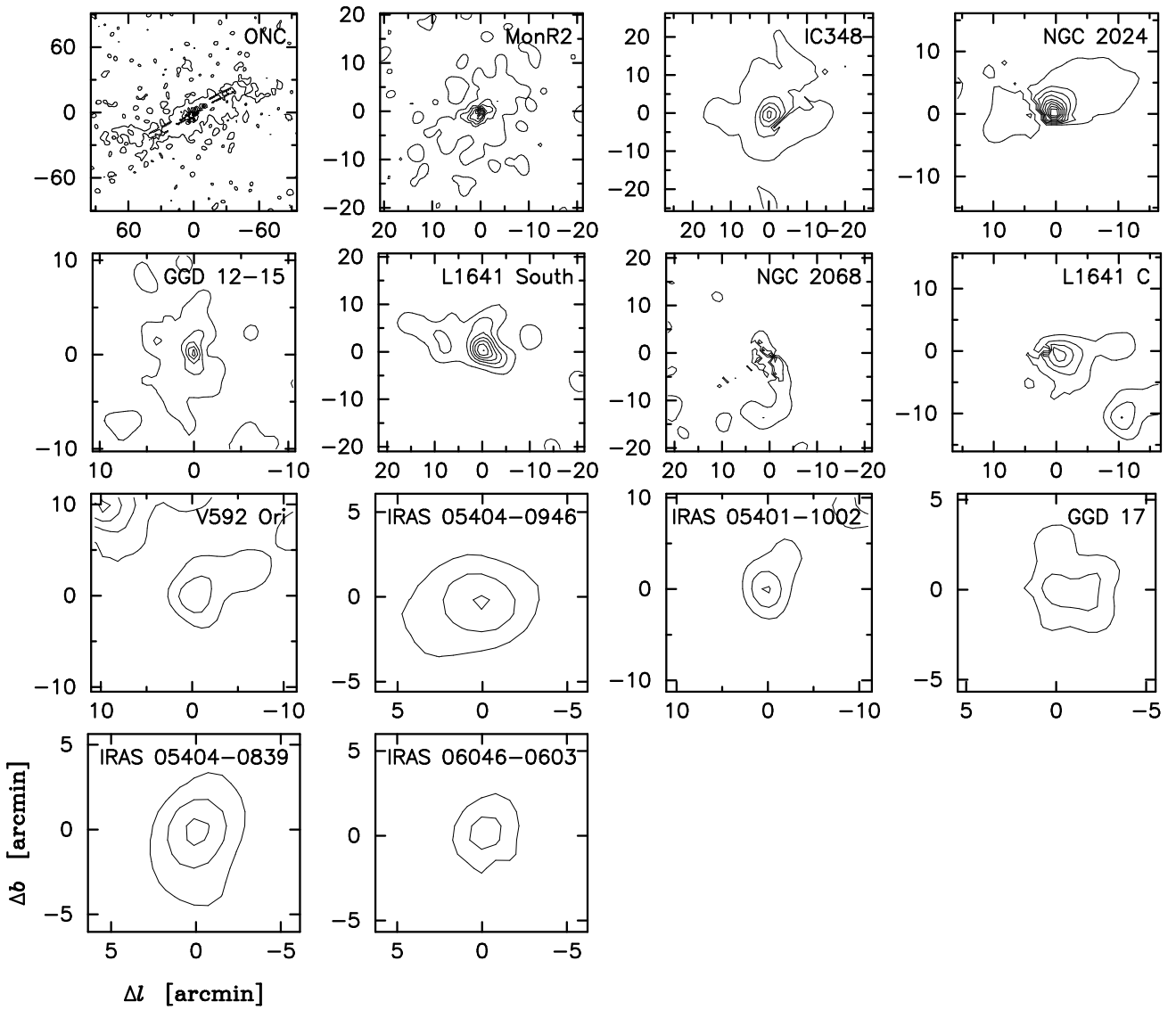


Fig. 8.— Contour maps of the  $K_s$  stellar surface density for each of the clusters summarized in Table 2 and labeled in Figures 4-7. Each contour map is centered on the cluster coordinates listed in Table 2. The angular size of the contour maps varies depending on the dimensions of the cluster. The contour levels in each map begin at  $2\sigma$  above the field star stellar surface density, where  $\sigma$  is the noise per pixel in the field surface density map estimated assuming Poisson statistics. The contour intervals are  $10\sigma$  for IC 348, ONC, NGC 2024, and MonR2, and  $3\sigma$  for the remaining clusters. The approximate noise level in field star surface density is  $\sigma \approx 0.1 \text{ arcmin}^{-2}$  for IC 348,  $\approx 0.15 \text{ arcmin}^{-2}$  for clusters in Orion, and  $\approx 0.3 \text{ arcmin}^{-2}$  for clusters in MonR2. Note that part of the cluster area in IC 348, L 1641 C, NGC 2024, and the ONC has been masked in the 2MASS Second Incremental Release Point Source Catalog to eliminate artifacts from bright stars. Also, the western portion of the NGC 2068 cluster has not been imaged with 2MASS at the time of this study.

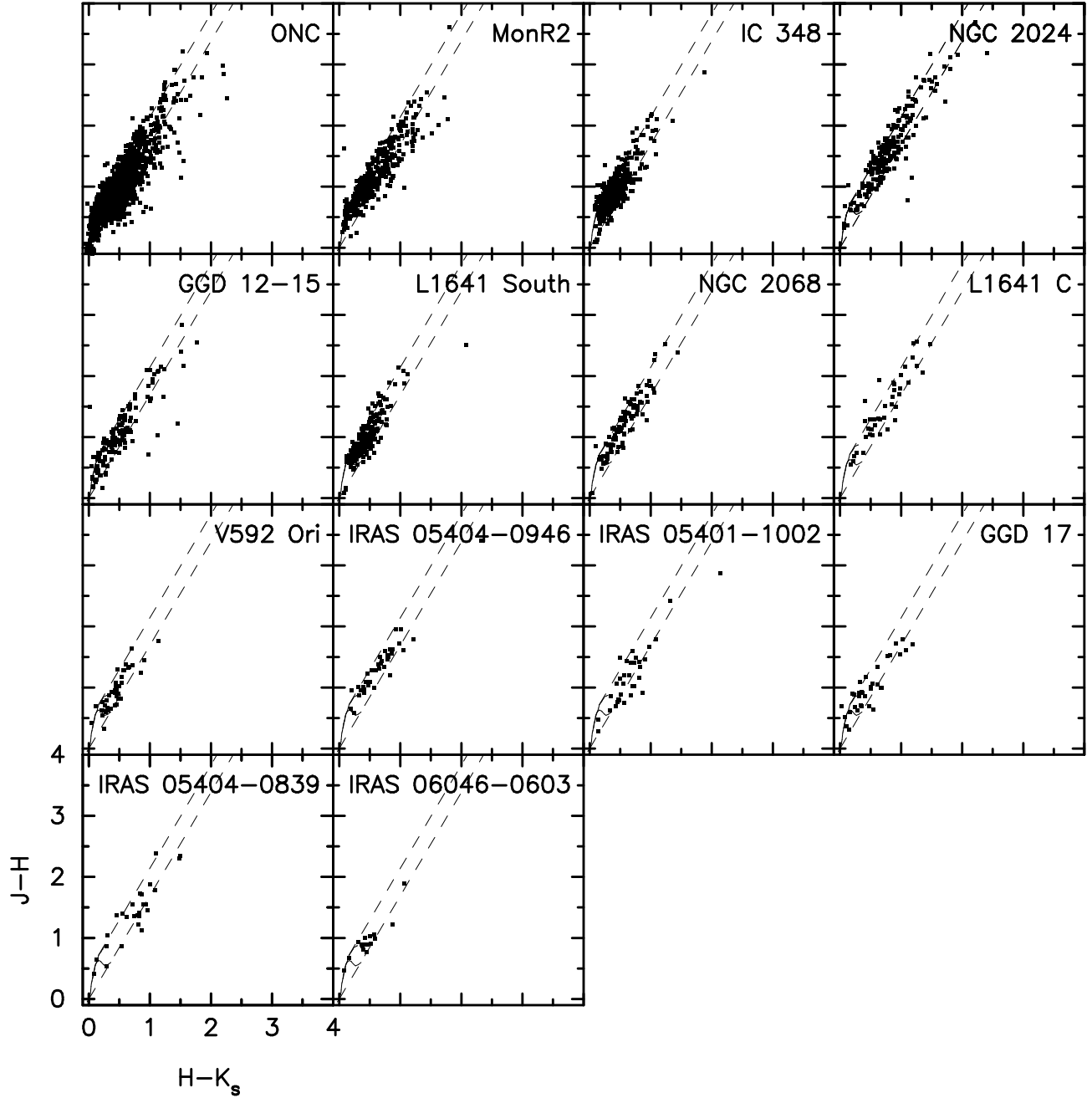


Fig. 9.—  $J - H$  vs  $H - K_s$  color-color diagram for each cluster identified in the  $K_s$  band stellar density maps. Only stars that have magnitudes of  $6.0^m \leq m(K_s) \leq 14.3^m$  and photometric uncertainties less than  $0.1^m$  in all three bands are shown. The solid curves show the locus of unreddened main sequence and giant stars in the CIT system (Bessell & Brett 1988), and the dashed lines show the reddening vectors from Cohen et al. (1981). Each cluster contains a number of red objects, supporting the notion that the clusters are indeed embedded within the molecular clouds.

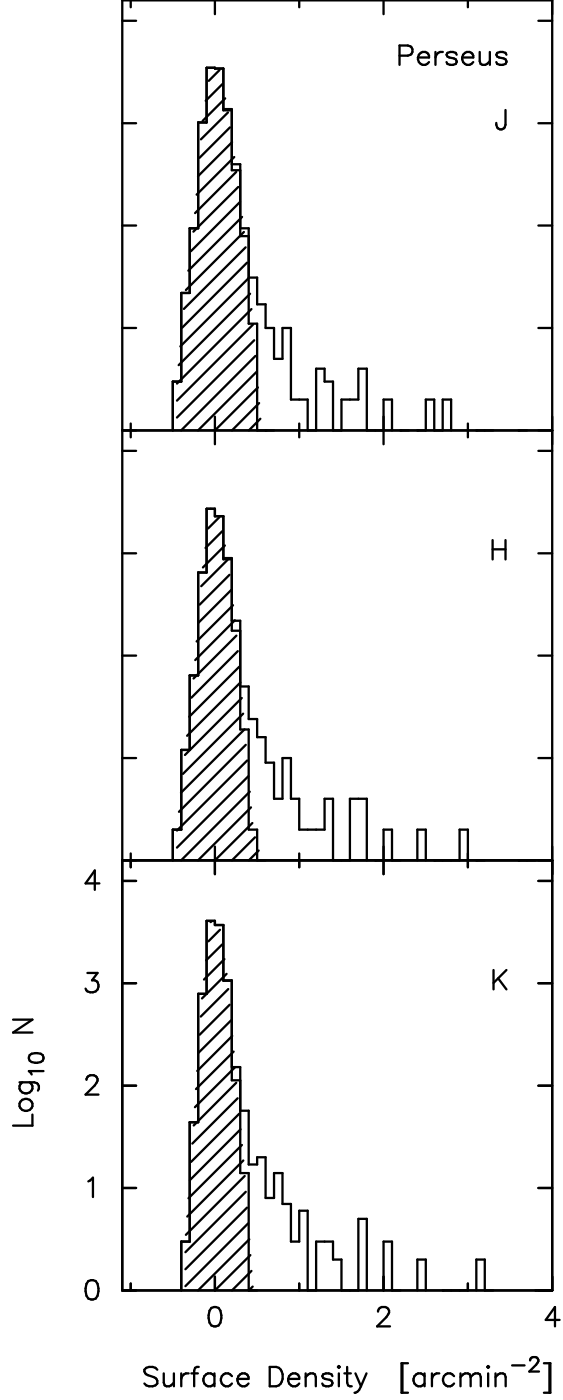


Fig. 10.— Histogram of the  $J$ ,  $H$ , and  $K_s$  stellar surface densities observed toward the Perseus molecular cloud after subtracting the nominal field star model. The open histograms are for all lines of sight toward the Perseus molecular cloud as defined by  $^{13}\text{CO}(1-0)$  emission. The hatched regions represent lines of sight outside the cluster boundaries but within the cloud area, and represent the surface density distribution of the distributed population. The mean surface density of the distributed population as inferred from the hatched histogram is summarized in Table 3.

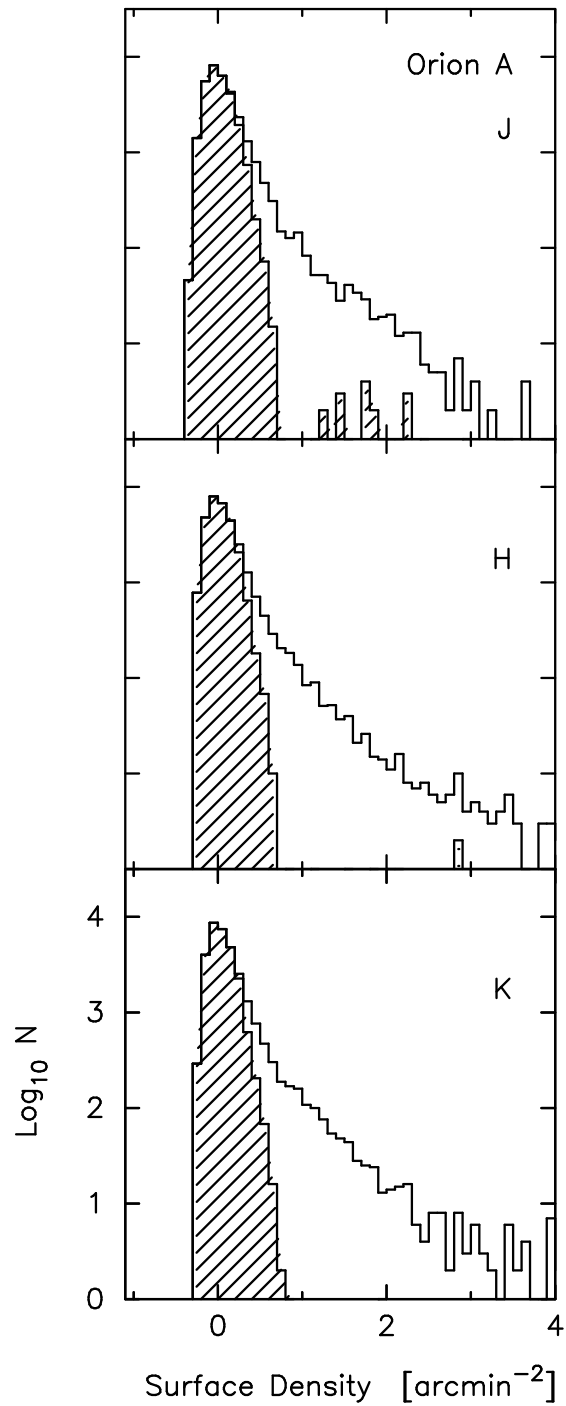


Fig. 11.— Same as Figure 10, except for the Orion A (L1641) molecular cloud.

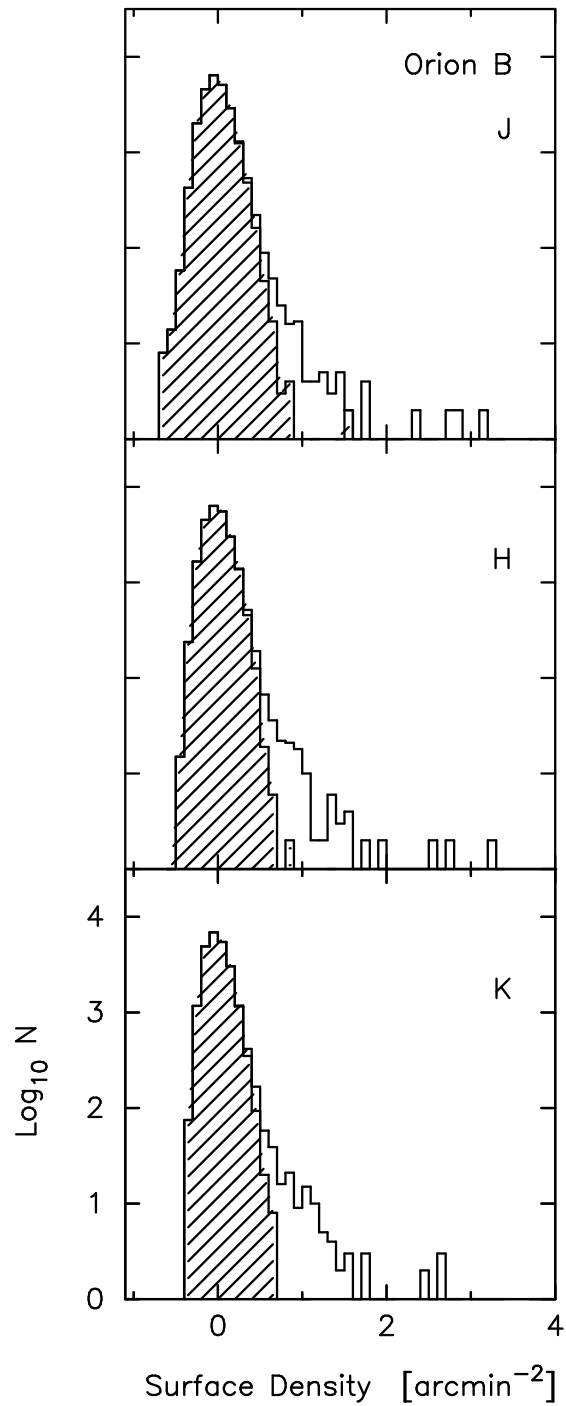


Fig. 12.— Same as Figure 10, except for the Orion B (L1630) molecular cloud.

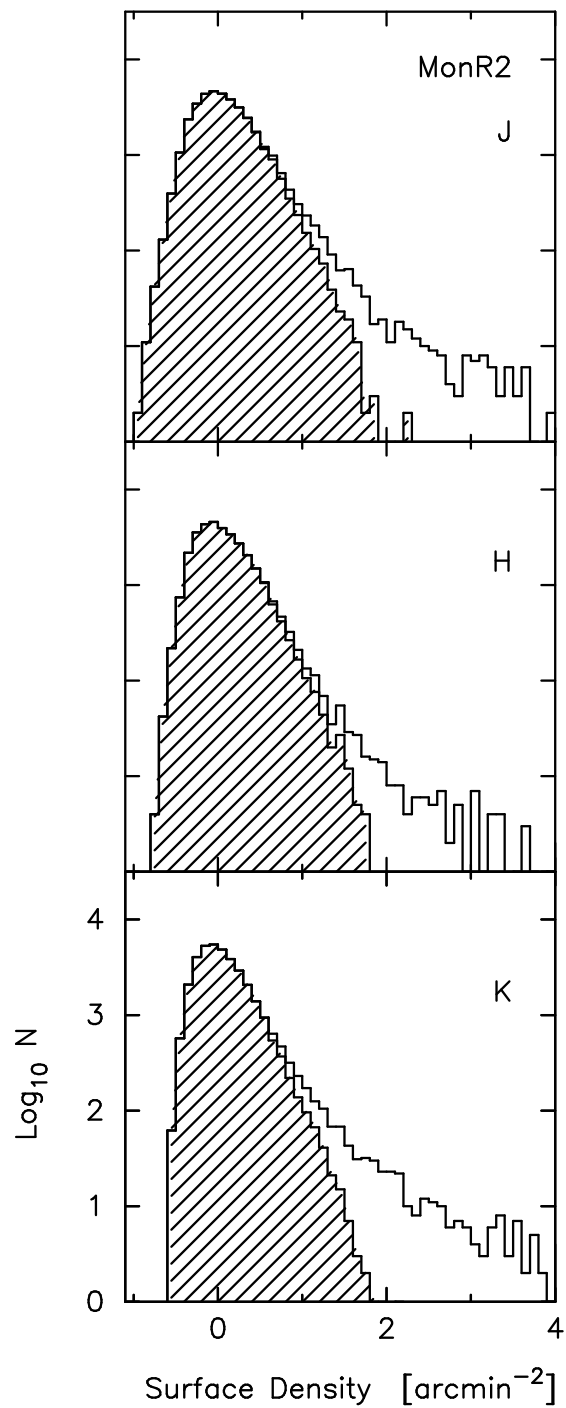


Fig. 13.— Same as Figure 10, except for the MonR2 molecular cloud.

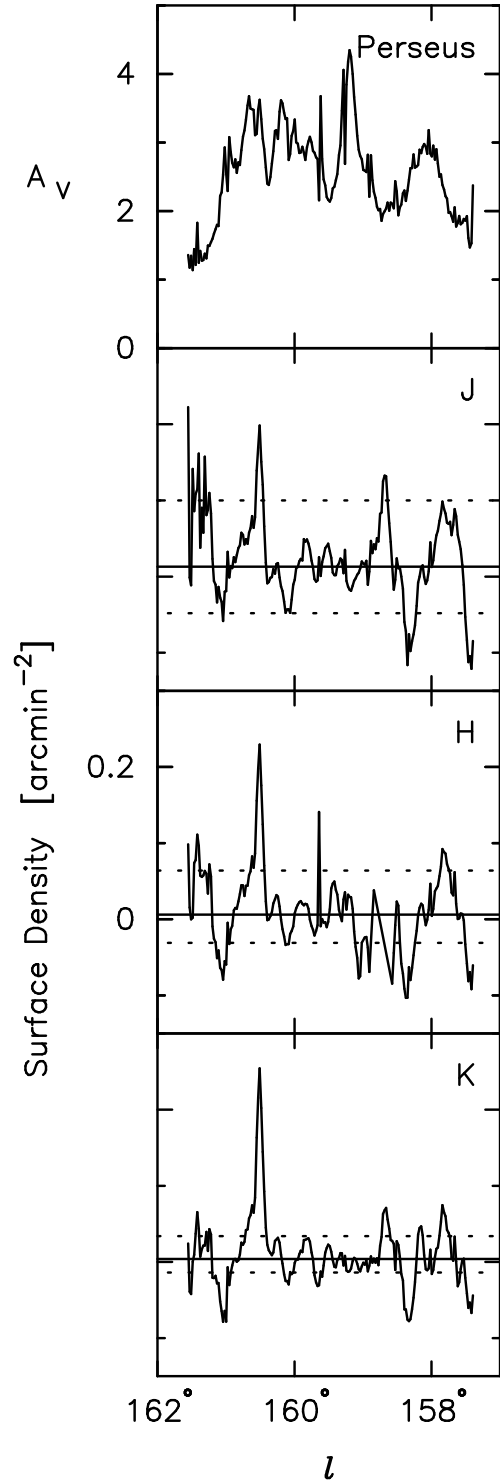


Fig. 14.— The visual extinction (top panel) and  $J$ ,  $H$ , and  $K_s$  band stellar surface density (bottom panels) as a function of Galactic longitude for the Perseus molecular cloud. The field stars have been subtracted from the star counts using the nominal extinction model, and the results averaged over Galactic latitude. The solid horizontal line shows the average surface density of the distributed population for the nominal extinction model, and the dashed horizontal lines show the inferred surface density assuming the low and high extinction models. This figure shows that the tightest constraints on the surface density of the distributed population is provided at  $K_s$  band where the field star subtraction is less sensitive to the assumed extinction model.

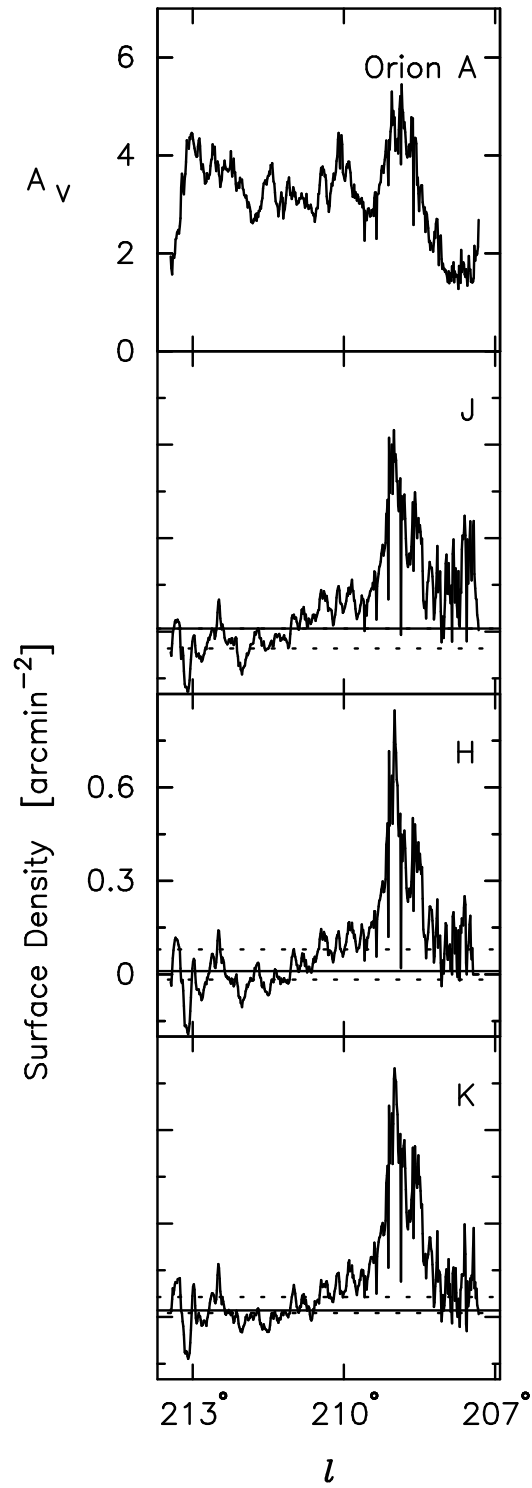


Fig. 15.— Same as in Figure 14, but for the Orion A molecular cloud.

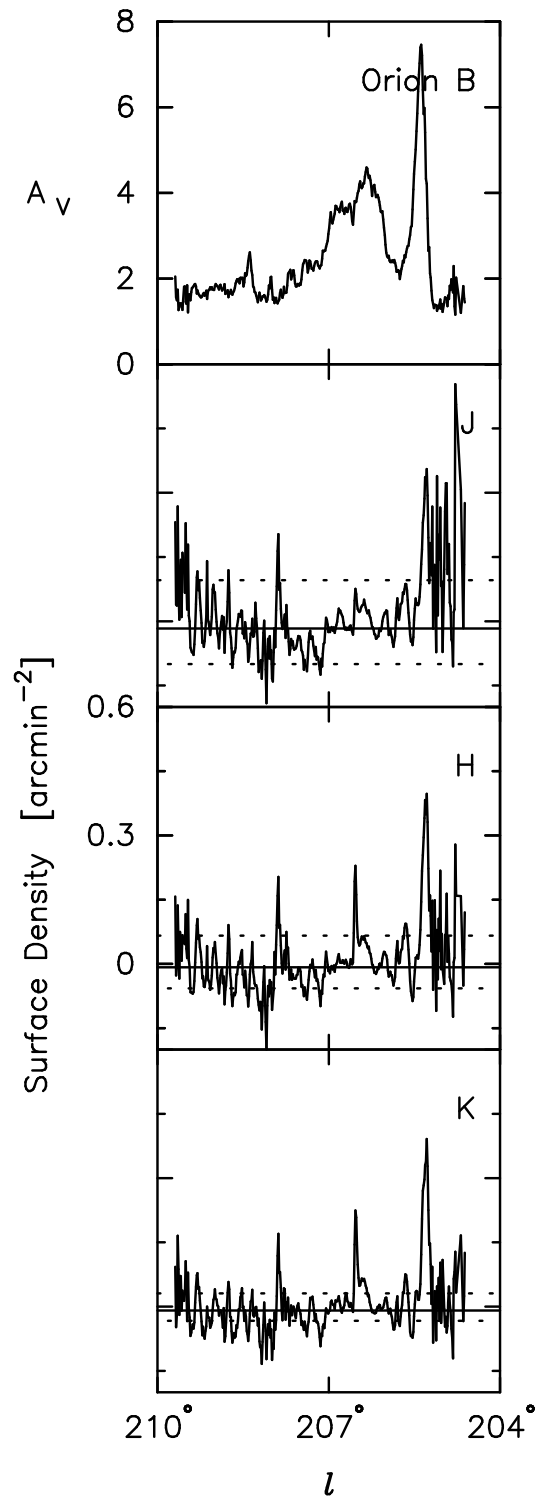


Fig. 16.— Same as in Figure 14, but for the Orion B molecular cloud.

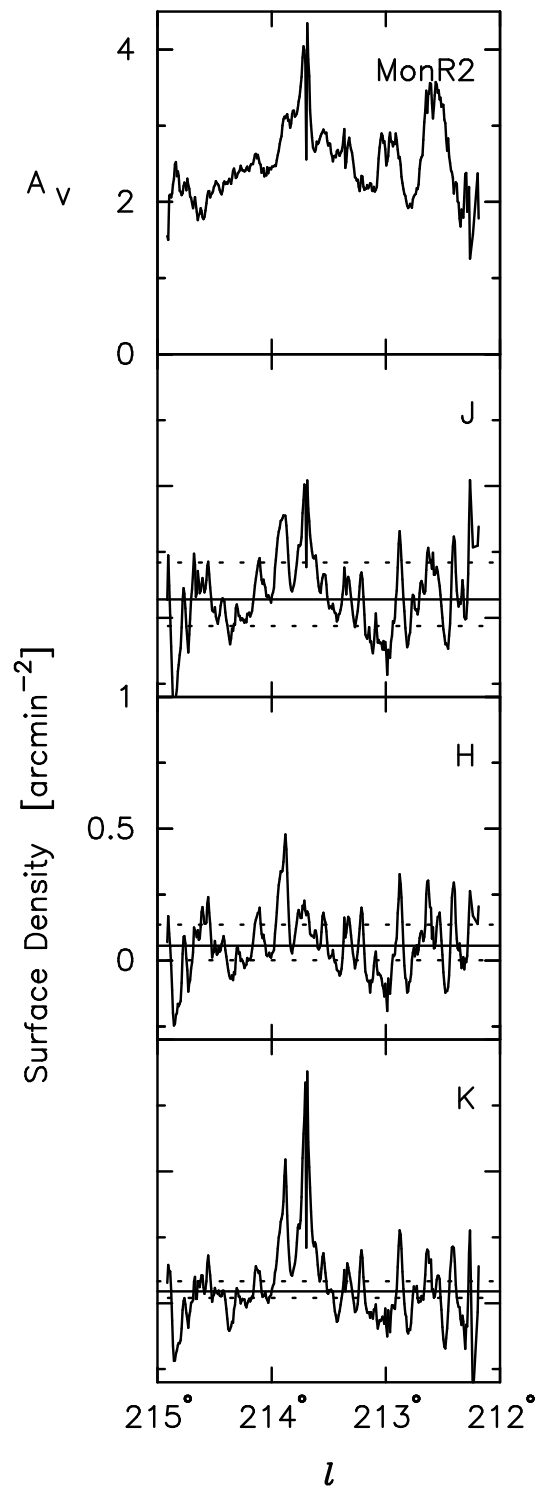


Fig. 17.— Same as in Figure 14, but for the MonR2 molecular cloud.

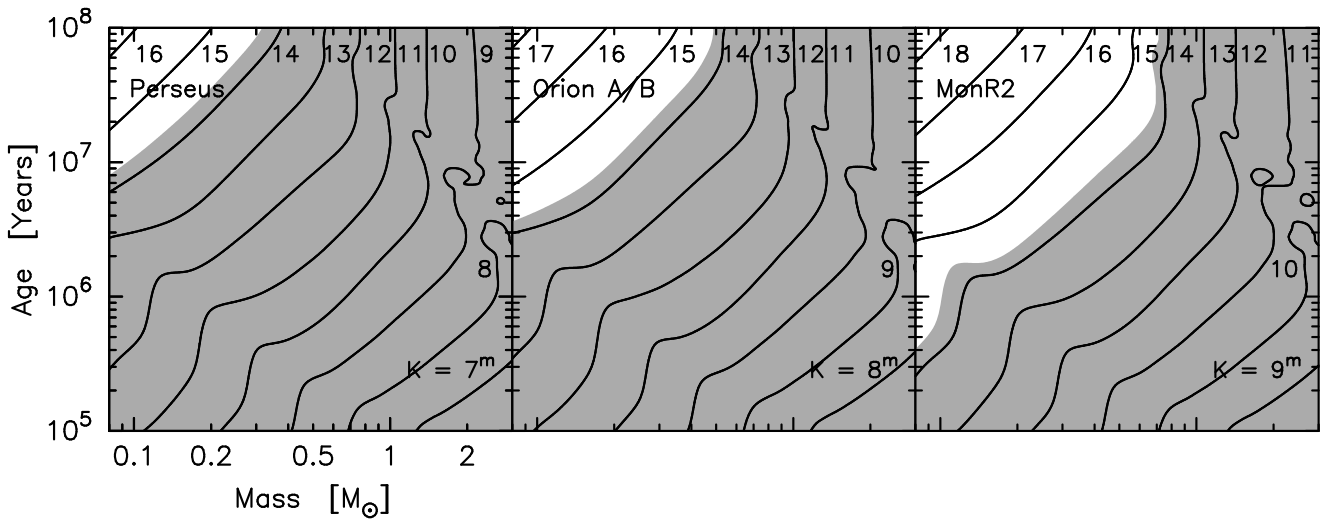


Fig. 18.—  $K_s$  band iso-magnitude contours as a function of stellar age and mass for stars at the distance of Perseus (320 pc), Orion A and Orion B (480 pc), and MonR2 (830 pc). The magnitudes were computed using the D'Antona & Mazzitelli (1997, 1998) pre-main-sequence evolutionary tracks assuming  $A_V = 0^m$  and that no near-infrared excess emission is present. The shaded area highlights the parameter space that is probed for the adopted  $K_s$  magnitude thresholds ( $6.0^m \leq m(K_s) \leq 14.3^m$ ).

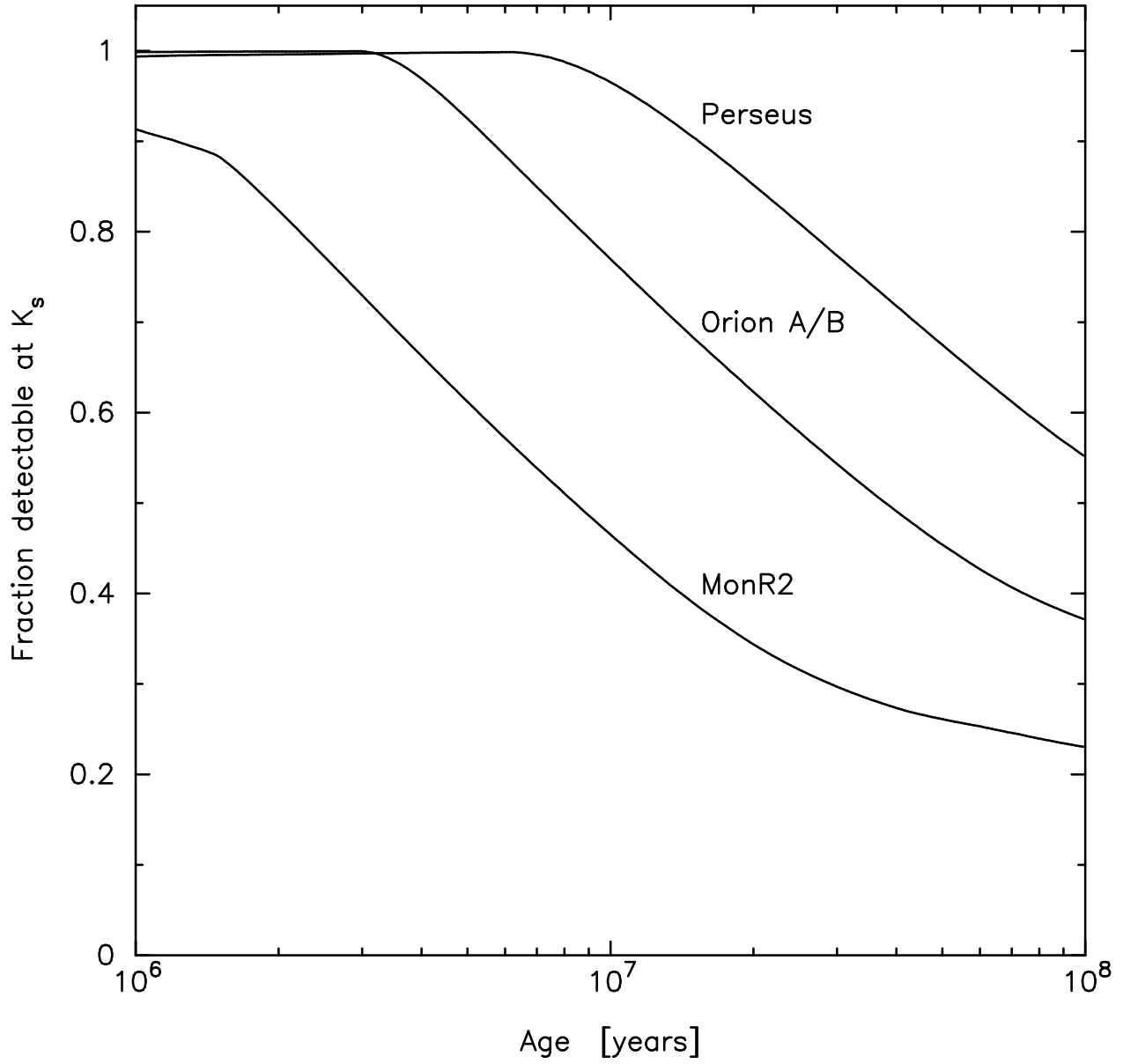


Fig. 19.— The fraction of a model stellar population with magnitudes of  $6.0^m \leq m(K) \leq 14.3^m$  as a function of the molecular cloud age for the Perseus, Orion A/B, and MonR2 molecular clouds. The model assumes that stars have been forming at a constant rate in time with a Miller-Scalo Initial Mass Function over the mass range of  $0.08-10 M_\odot$ , and that the visual extinction is the average value inferred from the  $^{13}\text{CO}$  maps ( $A_V \approx 3^m$ ). The magnitudes were computed using the D'Antona & Mazzitelli (1997, 1998) pre-main-sequence evolutionary tracks for objects with masses up to  $3 M_\odot$ , and assuming main sequence magnitudes for the more massive stars. The results indicate that the fraction of the model stellar population within the adopted  $K_s$  magnitude thresholds for ages  $< 100$  Myr ranges from  $> 67\%$  at the distance of Perseus to  $> 26\%$  at the distance of MonR2.

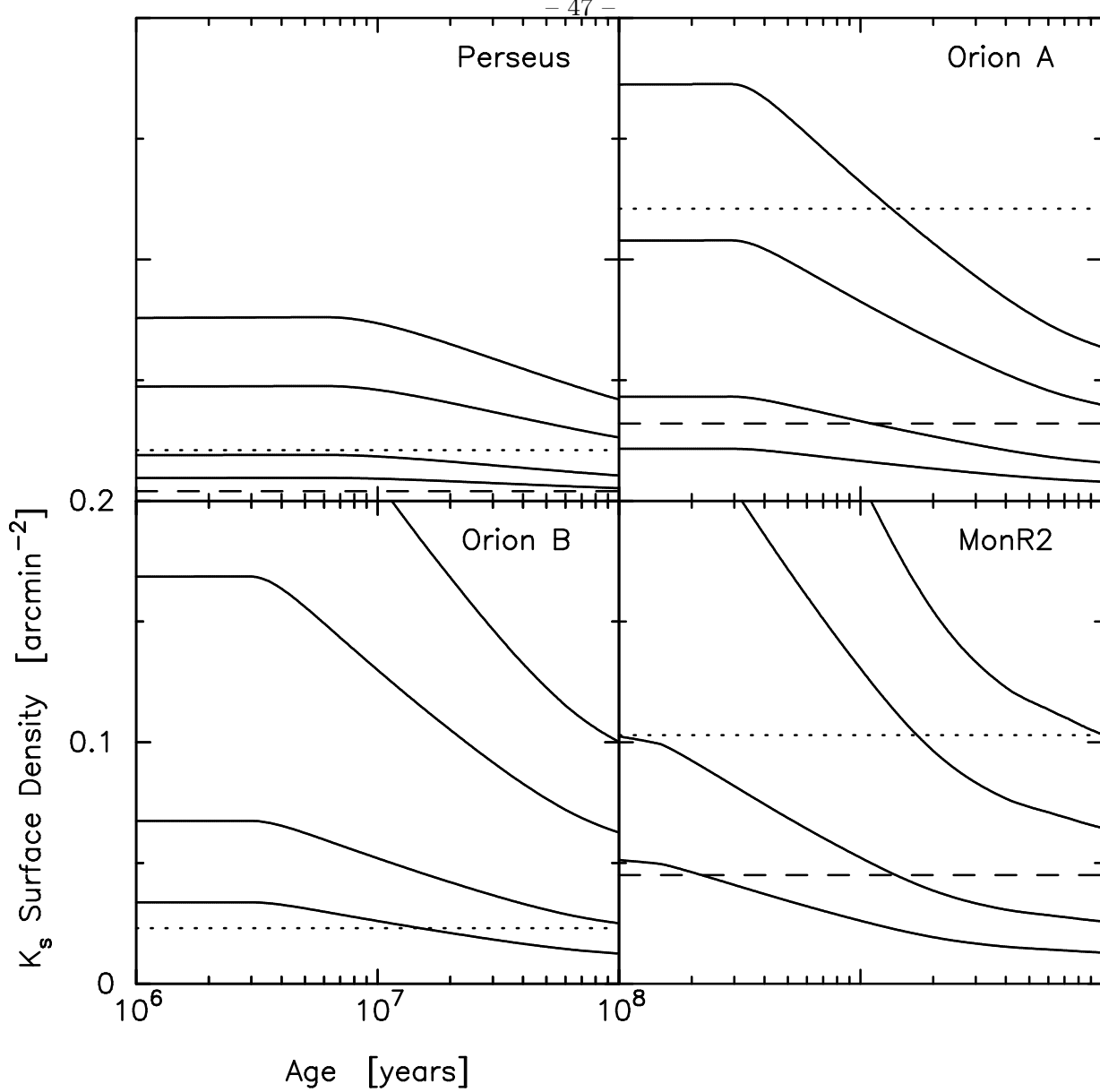


Fig. 20.— The predicted surface density of stars with apparent magnitudes of  $6.0^m \leq m(K) \leq 14.3^m$  as a function of the molecular cloud age for the Perseus, Orion A, Orion B, and MonR2 molecular clouds for the model calculations described in Figure 19. The solid curves are the predicted stellar surface density for an assumed star formation efficiency of 1% (bottom curves in each panel), 2%, 5%, and 8% (top curves in each panel) using the cloud masses implied by the nominal extinction model. The horizontal dashed line shows the inferred surface density for the distributed population (if a positive value; see Table 3), and the horizontal dotted line shows surface density for the clusters averaged over the entire cloud area. The older ages are intended to apply only to the distributed population. The global star formation efficiency implied by the sum of the cluster and distributed population ranges between  $\approx 2$  and 9% for the four clouds depending on the age assumed for the distributed population.

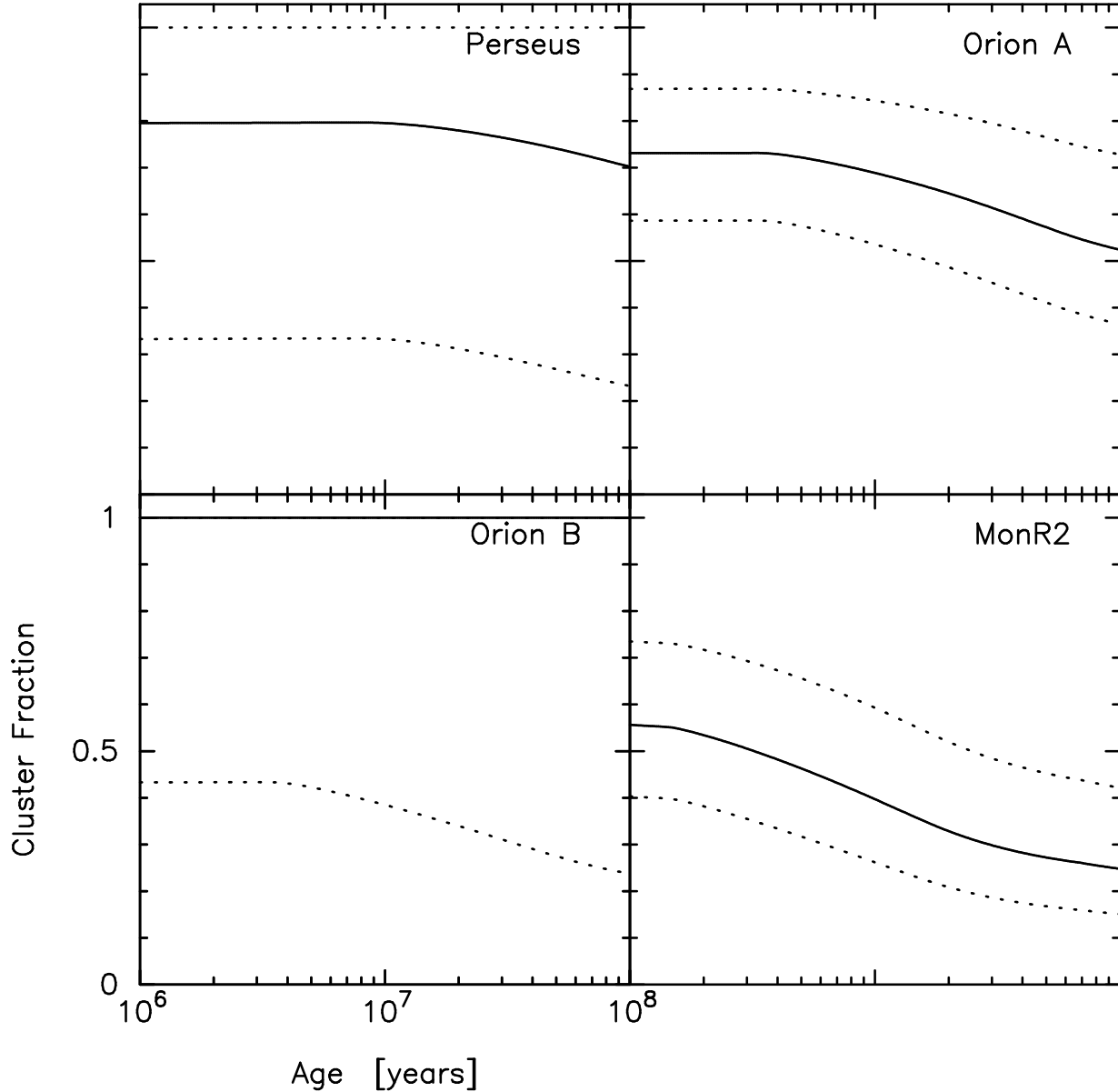


Fig. 21.— The fraction of the total stellar population currently contained in clusters as a function of the cloud age assuming that only part of the distributed population is detected at a given age as indicated by the model calculations shown in Figure 19. The solid lines show the fraction of stars in clusters for the nominal extinction model, and the dotted lines represent the low and high extinction models.

Table 1. Molecular Cloud Properties

Cloud	Coordinates		Distance [pc]	Area [deg <sup>2</sup> ]	Mass			References	
	$\ell$	$b$			Low	Nominal [10 <sup>4</sup> M <sub>⊙</sub> ]	High	Distance	<sup>13</sup> CO
Perseus	160	-19	320	6.4	1.0	1.3	1.9	1	4
Orion A	211	-20	480	6.2	2.5	3.3	4.8	2	5
Orion B	206	-15	480	7.2	2.4	3.2	4.7	2	6
MonR2	214	-13	830	2.6	2.3	3.1	4.6	3	6

References. —

- (1) de Zeeuw et al.(1999)
- (2) Genzel et al.(1981)
- (3) Herbst & Racine (1976)
- (4) Padoan et al.(1999)
- (5) Bally et al.(1987)
- (6) Miesch & Bally (1994)

Table 2. Stellar Clusters

ID	Galactic		Equatorial (J2000)		N <sub>stars</sub>	R <sub>eff</sub>	Comments
	$\ell$	$b$	$\alpha$	$\delta$			
<i>Perseus</i>							
1	160.5044	-17.8011	03:44:37.2	+32:09:19	>299	1.19	IC 348
<i>Orion A</i>							
2	208.9740	-19.3458	05:35:20.9	-05:20:29	>1744	3.86	Orion Nebula Cluster
3	210.8003	-19.5051	05:37:52.9	-06:57:09	23	0.56	V592 Ori
4	210.9800	-19.3276	05:38:49.6	-07:01:32	36	0.61	L1641 C
5	212.4710	-19.0181	05:42:27.1	-08:09:12	129	1.10	L1641 South
6	212.9816	-19.1469	05:42:50.1	-08:38:37	15	0.42	IRAS 05404-0839
7	214.0556	-19.6177	05:42:53.5	-09:45:38	23	0.47	IRAS 05404-0946
8	214.2706	-19.7824	05:42:38.4	-10:00:51	22	0.47	IRAS 05401-1002
<i>Orion B</i>							
9	205.3080	-14.2957	05:46:47.0	+00:06:16	>45	0.72	NGC 2068
10	206.5122	-16.3719	05:41:37.3	-01:53:39	>201	1.01	NGC 2024
<i>MonR2</i>							
11	213.3381	-12.6029	06:07:08.1	-06:03:53	15	0.41	IRAS 06046-0603
12	213.6955	-12.5926	06:07:47.8	-06:22:20	371	1.85	MonR2
13	213.8745	-11.8410	06:10:49.1	-06:11:38	134	1.13	GGD 12-15
14	214.1337	-11.4173	06:12:48.0	-06:13:56	23	0.61	GGD 17

Table 3. The Distributed Stellar Population

Cloud	Surface Density (arcmin <sup>-2</sup> )			N <sub>stars</sub>		
	Low	Nominal	High	Low	Nominal	High
Perseus						
<i>J</i>	-0.048	0.013	0.101	...	310	2300
<i>H</i>	-0.031	0.006	0.064	...	150	1500
<i>K<sub>s</sub></i>	-0.014	0.004	0.034	...	100	780
Orion A						
<i>J</i>	-0.054	0.009	0.099	...	210	2200
<i>H</i>	-0.017	0.021	0.080	...	470	1800
<i>K<sub>s</sub></i>	0.013	0.032	0.064	300	730	1400
Orion B						
<i>J</i>	-0.10	-0.018	0.096	...	...	2500
<i>H</i>	-0.057	-0.008	0.066	...	...	1700
<i>K<sub>s</sub></i>	-0.033	-0.009	0.031	...	...	790
MonR2						
<i>J</i>	-0.031	0.070	0.205	...	660	1900
<i>H</i>	0.001	0.056	0.136	10	530	1300
<i>K<sub>s</sub></i>	0.020	0.045	0.083	190	420	780

This figure "figure01.jpg" is available in "jpg" format from:

<http://arxiv.org/ps/astro-ph/0009118v1>

This figure "figure02.jpg" is available in "jpg" format from:

<http://arxiv.org/ps/astro-ph/0009118v1>

This figure "figure04.jpg" is available in "jpg" format from:

<http://arxiv.org/ps/astro-ph/0009118v1>

This figure "figure05.jpg" is available in "jpg" format from:

<http://arxiv.org/ps/astro-ph/0009118v1>

This figure "figure06.jpg" is available in "jpg" format from:

<http://arxiv.org/ps/astro-ph/0009118v1>

This figure "figure07.jpg" is available in "jpg" format from:

<http://arxiv.org/ps/astro-ph/0009118v1>